



Measurement of charged jet production cross sections and nuclear modification in p–Pb collisions at $\sqrt{s_{NN}} = 5.02$ TeV



ALICE Collaboration*

ARTICLE INFO

Article history:

Received 3 March 2015

Received in revised form 21 July 2015

Accepted 21 July 2015

Available online 26 July 2015

Editor: L. Rolandi

ABSTRACT

Charged jet production cross sections in p–Pb collisions at $\sqrt{s_{NN}} = 5.02$ TeV measured with the ALICE detector at the LHC are presented. Using the anti- k_T algorithm, jets have been reconstructed in the central rapidity region from charged particles with resolution parameters $R = 0.2$ and $R = 0.4$. The reconstructed jets have been corrected for detector effects and the underlying event background. To calculate the nuclear modification factor, R_{pPb} , of charged jets in p–Pb collisions, a pp reference was constructed by scaling previously measured charged jet spectra at $\sqrt{s} = 7$ TeV. In the transverse momentum range $20 \leq p_{T, \text{ch jet}} \leq 120$ GeV/c, R_{pPb} is found to be consistent with unity, indicating the absence of strong nuclear matter effects on jet production. Major modifications to the radial jet structure are probed via the ratio of jet production cross sections reconstructed with the two different resolution parameters. This ratio is found to be similar to the measurement in pp collisions at $\sqrt{s} = 7$ TeV and to the expectations from PYTHIA pp simulations and NLO pQCD calculations at $\sqrt{s_{NN}} = 5.02$ TeV.

© 2015 CERN for the benefit of the ALICE Collaboration. Published by Elsevier B.V. This is an open access article under the CC BY license (<http://creativecommons.org/licenses/by/4.0/>). Funded by SCOAP³.

1. Introduction

Jets are the observable final state of a fragmenting parton produced e.g. in scattering of partons in nuclei with a large momentum transfer, Q^2 . At sufficiently large Q^2 , the jet production cross section is computable since it can be factorized into the non-perturbative parton distribution and fragmentation functions and the cross section of partonic scatterings, which is calculable in perturbative QCD (pQCD) [1]. Jet measurements in p–Pb and their comparison to pp provide a tool to better constrain effects of (cold) nuclear matter on these factors. In particular, they can be used to examine the role of a modification of the initial distribution of quarks and gluons, e.g. shadowing effects and gluon saturation [2,3], and the impact of multiple scatterings and hadronic re-interactions in the initial and final state [4,5].

In central heavy-ion collisions, the production of jets and high- p_T particles is strongly modified: in Pb–Pb collisions at the LHC, the observed hadron yields are suppressed by up to a factor of seven compared to pp collisions, approaching a factor of two suppression at high p_T [6–8]. A similar suppression is also observed for reconstructed jets in central Pb–Pb [9–13]. This phenomenon, referred to as *jet quenching*, has also been observed previously in high- p_T particle production in central Au–Au collisions at RHIC [14–19]. It is attributed to the creation of a quark–gluon plasma (QGP) in the final state, where hard scattered partons radiate

gluons in strong interactions with the medium as first predicted in [20,21]. This results in a radiative energy loss of the leading parton and a modified fragmentation pattern.

Initially, p–Pb collisions have been seen as the testing ground for isolated cold nuclear matter effects, without the formation of a hot and dense medium. However, recent results on low- p_T particle production and long range correlations in p–Pb collisions at $\sqrt{s_{NN}} = 5.02$ TeV [22–25] exhibit features of collective behavior, similar to those found in Pb–Pb collisions, where they are attributed to the creation of a QGP. At high p_T , results on the production of unidentified charged particles [26–29] and jets [30,31] in p–Pb collisions at $\sqrt{s_{NN}} = 5.02$ TeV are consistent with the absence of a strong final state suppression. The question to what extent other nuclear effects lead to an enhancement of particle production at high p_T is still open, a possible enhancement in p–Pb collisions has been reported for single charged hadrons [28]. The measurement of jets in p–Pb collisions compared to single hadrons tests the parton fragmentation beyond the leading particle with the inclusion of low- p_T and large-angle fragments.

A jet is defined experimentally by the algorithm that combines the measured detector information such as tracks and/or calorimeter cells into jet objects and by the parameters of the algorithm. The desired properties of such algorithms in pp(\bar{p}) collisions and in the corresponding theoretical framework have been discussed e.g. in [32]. In general, jet algorithms aim to reconstruct the kinematic properties of the initial parton with as little dependence on the details of its fragmentation process as possible, i.e. the algorithms

* E-mail address: alice-publications@cern.ch.

should yield consistent results when applied in a theoretical calculation at any stage of a parton shower and at final state particle level. A particularly well suited class of algorithms in this context are those using sequential recombination schemes, which are infrared and collinear safe, in contrast to many conceptually simpler cone algorithms. The computationally optimized implementation of sequential recombination algorithms in the FastJet package [33] facilitates their applicability also in collision systems with high multiplicity and thereby the comparison of results obtained with the same jet algorithms in pp, p–Pb, and Pb–Pb collisions. An additional complication in the context of jet reconstruction in high-multiplicity events arises from the large background particle density, i.e. particles in the same aperture as the jet that are not related to the initial hard scattering. This background can be subtracted on an event-by-event basis and the impact on the reconstructed jet observable needs to be evaluated carefully [12,34,35].

In this paper, jets reconstructed from charged particles (*charged jets*) with the anti- k_T algorithm measured with the ALICE detector in p–Pb collisions at $\sqrt{s_{NN}} = 5.02$ TeV are reported for different resolution parameters, R . Section 2 describes in detail the correction steps needed in the analysis, including the effect of the event background and its fluctuations on the jet observables and the unfolding procedure to account for background as well as detector effects. The results are presented and discussed in Section 3.

2. Data analysis

2.1. Event and track selection

The data used for this analysis were taken with the ALICE detector [36] during the p–Pb run of the LHC at $\sqrt{s_{NN}} = 5.02$ TeV at the beginning of 2013. Minimum bias events have been selected requiring at least one hit in both of the scintillator trigger detectors (VOA and VOC) covering the pseudorapidity $2.8 < \eta_{lab} < 5.1$ and $-3.7 < \eta_{lab} < -1.7$, respectively [37]. Here and in the following, η_{lab} denotes the pseudorapidity in the ALICE laboratory frame. Compared to this frame (with positive η in the direction of the VOA), the nucleon–nucleon center-of-mass system moves in rapidity by $y_{NN} = -0.465$ in the direction of the proton beam [38].

The event sample used in the analyses presented in this manuscript was collected exclusively for the beam configuration where the proton travels from VOA to VOC (clockwise). A van der Meer scan was used to measure the visible cross section $\sigma_{VO} = 2.09 \pm 0.07$ b for this case [39]. Monte Carlo studies show that the sample consists mainly of non-single diffractive (NSD) interactions and a negligible contribution from single diffractive and electromagnetic interactions (for more details see [38,40]). The trigger is not fully efficient for NSD events. This inefficiency affects only events without a reconstructed vertex, i.e. with no particles reconstructed within the acceptance of the SPD. The loss of efficiency is estimated to be 2.3% with a large systematic uncertainty of 3.1% [38]. In this paper, the normalization to NSD events is only used for the construction of the nuclear modification factor.

In addition to the trigger selection, timing and vertex-quality cuts are used to suppress pile-up and bad quality events. The analysis requires a reconstructed vertex, which is the case for 98.2% of the events selected by the trigger. In addition, events with a reconstructed vertex $|z| > 10$ cm along the beam axis are rejected. In total, about 96M events are used for the analysis.

Charged particles are reconstructed as tracks in the Inner Tracking System (ITS) [41] and the Time Projection Chamber (TPC) which cover the full azimuth and $|\eta_{lab}| < 0.9$ [42]. For tracks with reconstructed track points close to the vertex (from the two inner Silicon Pixel Detector (SPD) layers of the ITS), a momentum resolution of 0.8% (3.8%) for $p_T = 1$ GeV/c (50 GeV/c) is reached [36].

The azimuthal distribution of these high quality tracks is not completely uniform due to inefficient regions in the SPD. This can be compensated by considering in addition tracks *without* reconstructed track points in the SPD. For those tracks, the primary vertex is used as an additional constraint in the track fitting to improve the momentum resolution. This approach yields a very uniform tracking efficiency within the acceptance, which is needed to avoid geometrical biases of the jet reconstruction algorithm caused by a non-uniform density of reconstructed tracks. The procedure is described in detail in the context of jet reconstruction with ALICE in Pb–Pb events [12]. For the analyzed data, the additional tracks (without SPD track points) constitute approximately 4.3% of the used track sample. Tracks with $p_T > 0.15$ GeV/c and within a pseudorapidity interval $|\eta_{lab}| < 0.9$ are used as input to the jet reconstruction. The overall efficiency for charged particle detection, including the effect of tracking efficiency as well as the geometrical acceptance, is 70% at $p_T = 0.15$ GeV/c and increases to 85% at $p_T = 1$ GeV/c and above.

2.2. Jet reconstruction and background corrections

For the present analysis, the anti- k_T algorithm from the FastJet package [43] has been used to reconstruct jets from measured tracks with resolution parameters of $R = 0.2$ and $R = 0.4$. In general, jets are only considered for further analysis if the jet-axis is separated from the edge of the track acceptance in η_{lab} by at least the resolution parameter R used in the jet finding, e.g. jets reconstructed with $R = 0.4$ are accepted within $|\eta_{jet, lab}| < 0.9 - 0.4 = 0.5$. The jet transverse momentum is calculated by FastJet using the p_T recombination scheme. To enable background corrections, the area A for each jet is determined internally by distributing *ghost particles* into the area that is clustered [44]. Ghost particles have vanishing momentum and therefore do not influence the jet finding procedure. By construction, the number of ghost particles in a jet is a direct measure for the jet area. A ghost particle density of 200 per unit area (0.005 area per ghost particle) was used to obtain a good area resolution with a reasonable computing time.

In Pb–Pb collisions, the background from particles not from the same hard scattering as the jet has a significant impact on the reconstructed jet momentum [12,35]. The transverse momentum density of this background is estimated with a statistically robust method by using the median of all jet $p_{T, ch jet}$ per area within one event for jets reconstructed with the k_T algorithm. In p–Pb collisions, the multiplicity density is two orders of magnitude smaller than in central Pb–Pb collisions [40], so a corresponding reduction of the jet background is expected. To obtain a reliable estimate for the more sparse environment of p–Pb events a modified version of the approach described in [45] for pp collisions is employed. It uses the same method as in Pb–Pb, but contains an additional correction factor, C , to account for regions without particles, which otherwise would not contribute to the overall area estimate. The background density for each event is then given by

$$\rho_{ch} = \text{median} \left\{ \frac{p_{T,i}}{A_i} \right\} \cdot C, \quad (1)$$

where i runs over all reconstructed k_T jets in the event with momentum $p_{T,i}$ and area A_i . C is defined by

$$C = \frac{\sum_j A_{j, k_T}}{A_{acc}}. \quad (2)$$

Here, the numerator is the area of all k_T jets containing tracks and the denominator, A_{acc} , is the acceptance in which charged particles are considered as input to the jet finding ($2 \times 0.9 \times 2\pi$). The probability distribution for the background density in this method,

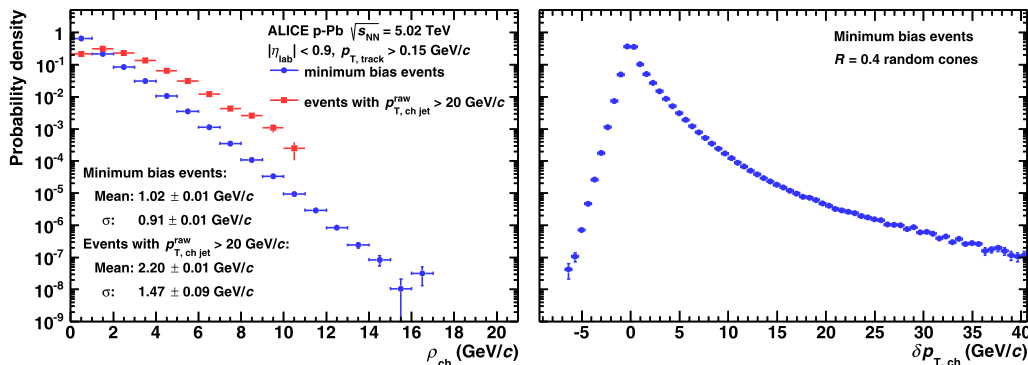


Fig. 1. (Color online.) Left: Probability distribution of the event-by-event transverse momentum background density (see Eq. (1)). The mean and variance for two event classes are indicated in the figure. $p_{T, ch jet}^{raw}$ represents uncorrected jet p_T . Right: Probability distribution of background fluctuations calculated with the random cone approach and defined via Eq. (4) (resolution parameter $R = 0.4$).

with the same track selection criteria as the signal jet reconstruction and a radius of 0.4, is shown in Fig. 1 (left). The background density obtained with $R = 0.4$ is used both for the correction of signal jets with $R = 0.4$ and $R = 0.2$ to avoid event-by-event fluctuations in the difference of the momenta for the two radii.

The probability distribution of ρ_{ch} decreases approximately exponentially. It is smaller than 4 GeV/c for 98.6% of all events. The mean background density and its variance for all events is $\langle \rho_{ch} \rangle = 1.02$ GeV/c (with negligible statistical uncertainty) and $\sigma(\rho_{ch}) = 0.91 \pm 0.01$ GeV/c. For events containing a jet with uncorrected transverse momentum $p_{T, ch jet} > 20$ GeV/c, it is $\langle \rho_{ch} \rangle = 2.20 \pm 0.01$ GeV/c and $\sigma(\rho_{ch}) = 1.47 \pm 0.09$ GeV/c, respectively. The observed increase of the underlying event activity for events that contain a high- p_T jet is expected. This increase is already present in pp collisions and has been quantified in detail and with more differential observables than the background density, e.g. in [46].

The background density estimate provides an event-by-event correction for each jet with reconstructed transverse momentum $p_{T, ch jet}$ and jet area $A_{ch jet}$:

$$p_{T, ch jet} = p_{T, ch jet}^{raw} - A_{ch jet} \cdot \rho_{ch}. \quad (3)$$

However, this approach neglects that the background for a given event is not uniformly distributed in the (η_{lab}, φ) -plane but fluctuates from region to region. These fluctuations are mainly Poissonian, but also encode correlated region-to-region variations of the particle multiplicity and the mean p_T [35]. The effect of these fluctuations can be accounted for on a statistical basis in the unfolding of the measured jet $p_{T, ch jet}$ -distributions. The distribution of region-to-region density fluctuations around the event-wise background density estimate can be evaluated for the full event sample by a *Random Cone* (RC) approach as described in [35]. Cones with a radius R corresponding to the resolution parameter of the jet finding algorithm are placed randomly in the (η_{lab}, φ) jet-acceptance and the transverse momenta for all tracks (charged particles) falling into this cone are summed and compared to the background estimate:

$$\delta p_{T, ch} = \sum_i p_{T, i} - \rho_{ch} A, \quad A = \pi R^2. \quad (4)$$

The distribution of the residuals, $\delta p_{T, ch}$, as shown in Fig. 1 (right) for $R = 0.4$, is a direct measure for all intra-event fluctuations of the background and can be used directly in the unfolding procedure. In Fig. 1 (right), a clear asymmetry of the distribution is visible. It is caused by the fact that the $\delta p_{T, ch}$ distribution of single particles sampled in the cone is asymmetric. Since the number of particles within a cone increases with its size, statistical fluctuations of the background estimate also increase (see also [35]).

Furthermore, the randomly placed cones can also overlap with jets. In p-Pb collisions, there is the possibility for multiple hard collisions within one p-Pb event, so a jet can also be the background to a jet from another hard collision and contribute as an upward fluctuation. Therefore, an overlap of random cones with possible signal jets should not be *a priori* excluded in the fluctuation estimate, but is part of its systematic uncertainty.

2.3. Detector effects and unfolding

The main detector-related effects on the reconstructed jet are the reconstruction efficiency and the momentum resolution for these, a full detector simulation of pp jet events generated with PYTHIA6 (Perugia 2011, version 6.425) [47] and GEANT3 particle transport [48] is performed. In the simulation, two jet collections are matched geometrically (closeness in (η_{lab}, φ) -plane) with a one-to-one correspondence [12]: jets reconstructed at the charged particle level (*part*) without detector effects and jets reconstructed from tracks after particle transport through the ALICE detector (*det*). In the simulation, the particle level reconstruction includes charged primary particles produced in the collision with $p_T > 0.15$ GeV/c. Charged decay products from primary particle decays, excluding those from weak decays of strange particles, are included with the same p_T threshold. The response matrix is populated with matched particle- and detector-level jets. It relates the particle-level to the detector-level charged jet momentum and encodes the effects of single-particle momentum resolution and reconstruction efficiency on the reconstructed jet momentum. A correction for the missing energy of neutral jet-constituents is not applied. The response is shown on a logarithmic scale in Fig. 2 (left) for charged jets with $R = 0.4$ and particle-level momentum between $45 < p_{T, ch jet}^{part} < 50$ GeV/c. It can be seen that the most probable value for the reconstructed momentum is the particle-level momentum, but the distribution has large tails to the left and right. It is more probable that jets are reconstructed with a lower momentum than the truth, which is due to the dominating effect of the single-particle reconstruction efficiency that reduces the number of reconstructed particles in a jet. The tail to the right-hand side is mainly due to the single-particle momentum resolution, where a fraction of tracks is reconstructed with higher momentum than the truth, causing an upward shift of the jet momentum.

In addition, Fig. 2 (left) shows the effect of the background fluctuations on the reconstructed jet momentum and the combination of detector effects and background fluctuations. Even though the background fluctuations show a strong tail to the right-hand side, it is seen that in the combined unfolding matrix the effects

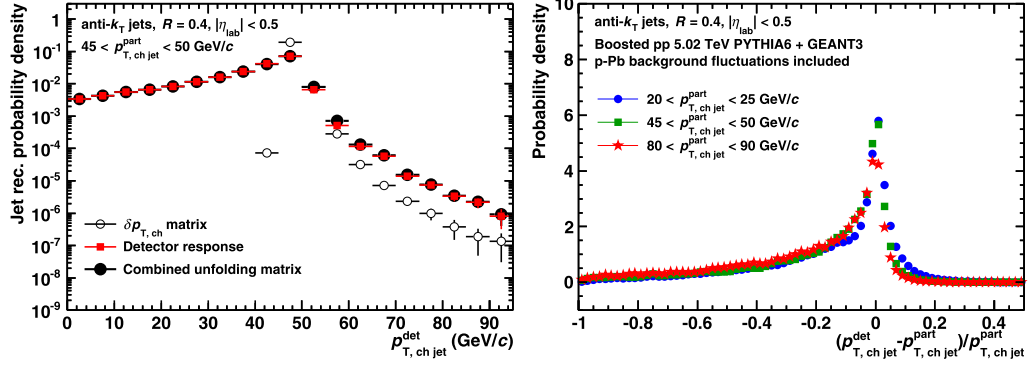


Fig. 2. (Color online.) Left: Projection of the combined unfolding matrix for jets with particle-level momentum $45 < p_{T, \text{ch jet}}^{\text{part}} < 50 \text{ GeV}/c$. The matrix is obtained from the combination of the detector response and background fluctuation matrices, which are also shown as projections (see text for details). Right: Probability distribution of the relative difference between particle-level (generated true) and detector-level charged jet transverse momentum for jets with different momenta. The effect of background fluctuations is included for the jets reconstructed at detector level. Characteristic values of the distributions are summarized in Table 1.

Table 1

Characteristic values for the distribution of residuals of the total charged jet response shown in Fig. 2 (right), including the effect of background fluctuations and without: most probable value (MPV) determined via a Gaussian fit to the central peak region, first and second moment (mean and width σ), and quartiles. The precision of the quartiles is limited by the finite bin width of 0.01.

$p_{T, \text{ch jet}}^{\text{part}}$	20–25 GeV/c	45–50 GeV/c	80–90 GeV/c
MPV (Gaussian fit)	0.006 ± 0.002	-0.001 ± 0.002	-0.010 ± 0.004
id. w/o bkg. fluct.	0.007 ± 0.001	-0.003 ± 0.002	-0.013 ± 0.004
Mean	0.149 ± 0.030	-0.181 ± 0.030	-0.222 ± 0.030
id. w/o bkg. fluct.	-0.163 ± 0.030	-0.188 ± 0.030	-0.226 ± 0.030
Width σ	0.238 ± 0.030	0.246 ± 0.030	0.259 ± 0.030
id. w/o bkg. fluct.	0.233 ± 0.009	0.245 ± 0.005	0.258 ± 0.003
Quartile, 25% above	0.01 ± 0.01	-0.01 ± 0.02	-0.01 ± 0.02
id. w/o bkg. fluct.	0.01 ± 0.01	-0.01 ± 0.02	-0.03 ± 0.02
Quartile, 50% above	-0.05 ± 0.04	-0.09 ± 0.01	-0.13 ± 0.04
id. w/o bkg. fluct.	-0.07 ± 0.04	-0.09 ± 0.04	-0.13 ± 0.04
Quartile, 75% above	-0.25 ± 0.06	-0.29 ± 0.05	-0.37 ± 0.04
id. w/o bkg. fluct.	-0.27 ± 0.04	-0.29 ± 0.06	-0.37 ± 0.04

of single-particle momentum resolution play the dominant role in reconstructing a jet with momentum higher than the truth. The default algorithm for the unfolding of the measured jet spectrum is based on the *Singular Value Decomposition* (SVD) approach [49] as implemented in the RooUnfold package [50]. The default prior in the unfolding procedure is a smoothed version of the uncorrected jet spectrum itself. In addition to the SVD unfolding approach, Bayesian [51,52] and χ^2 [53] unfolding have been used for systematic comparisons and validity checks. The unfolded spectrum is also corrected for unmatched jets using a jet reconstruction efficiency obtained from generated-reconstructed comparison. This jet reconstruction efficiency is larger than 96% in the considered momentum range.

The influence of these detector effects and background fluctuations on the jet momentum is shown for three transverse momentum intervals in Fig. 2 (right) via the probability distribution of the relative difference of the detector-level and particle-level charged jet transverse momentum. For all momentum bins the distribution is asymmetric. The most probable response was determined using Gaussian fits to the peak region. It can be seen in Table 1 that it is close to zero ($\leq 1\%$) with a mild p_T dependence. To further quantify the distributions, numerical values for their mean and width are also given in Table 1. Since the width is not a well-defined measure of the jet momentum resolution for these asymmetric distributions, the quartiles of the distribution are provided in addition. Approximately, 25% of the jets have a larger momentum than the generated. The 50% (median) correction is only 5% for $p_{T, \text{ch jet}}^{\text{part}} = 20\text{--}25 \text{ GeV}/c$ and increases towards larger jet momenta.

In Table 1 the values for the respective distributions without background fluctuations are also given (not shown in Fig. 2). Clearly, the instrumental response dominates the jet response as already seen in Fig. 2 (left). The main effect of the background fluctuations is a broadening of the jet response and an upward shift of the average reconstructed energy due to the asymmetric shape of the fluctuations as seen in Fig. 1 (right). The most probable value remains unaffected within the uncertainties when background fluctuations are included.

2.4. Nuclear modification factor

The nuclear modification factor compares a p_T -differential yield in p–Pb collisions to the differential production cross section in pp collisions at the same $\sqrt{s_{\text{NN}}}$ to quantify nuclear effects:

$$R_{\text{pPb}} = \frac{d^2 N_{\text{pPb}}/d\eta dp_T}{\langle T_{\text{pPb}} \rangle \cdot d^2 \sigma_{\text{pp}}/d\eta dp_T}. \quad (5)$$

Here, $\langle T_{\text{pPb}} \rangle$ is the nuclear overlap function which accounts for the increased parton flux in p–Pb compared to pp collisions. It is related to the number of binary nucleon–nucleon collisions via $\langle T_{\text{pPb}} \rangle = \langle N_{\text{coll}} \rangle / \sigma_{\text{INEL}}^{\text{pp}}$ and has been calculated in a Glauber Monte Carlo, as described in [38]. Here, $\sigma_{\text{INEL}}^{\text{pp}}$ represents the total inelastic cross section in pp collisions. For minimum bias p–Pb collisions, the nuclear overlap function is $\langle T_{\text{pPb}} \rangle = (0.0983 \pm 0.0034) \text{ mb}^{-1}$ and $\langle N_{\text{coll}} \rangle = 6.87 \pm 0.56$. In this paper, the reference differential production cross section in pp is constructed from the ALICE charged jet measurement at 7 TeV [54] by a pQCD based scaling. In the nuclear modification factor, the invariant yield for NSD events in p–Pb is compared to inelastic pp collisions. Hence, the additional correction of $(2.3 \pm 3.1)\%$ is applied as discussed above.

2.5. NLO calculations and pp reference

Perturbative QCD calculations are used for two purposes in this paper: for comparison to the measurement of jet production in p–Pb, and as additional input to the construction of the pp reference. The calculations have been performed within the POWHEG box framework [55,56], which facilitates next-to-leading order (NLO) precision in calculating parton scattering cross sections in an event-by-event Monte Carlo. Event-by-event the outgoing partons from POWHEG are passed to PYTHIA8 [57] where the subsequent parton shower is handled. For this, a POWHEG version matched to the PYTHIA8 fragmentation is used to avoid double counting of NLO effects already considered in the PYTHIA8 code. The Monte Carlo approach has the advantage that the same

Table 2
Summary of systematic uncertainties on the fully corrected jet spectrum, the corresponding nuclear modification factor, and the jet production cross section ratio for the resolution parameters $R = 0.2$ and $R = 0.4$. The percentages are given for the whole shown transverse momentum range 20–120 GeV/c.

Observable Resolution parameter	Jet cross section		R_{pPb}		\mathcal{R} 0.2/0.4
	$R = 0.2$	$R = 0.4$	$R = 0.2$	$R = 0.4$	
<i>Uncertainty source</i>					
Single-particle efficiency (%)	7.9–12.8	10.2–14.2	4.1–5.9	4.9–6.3	2.1–2.1
Unfolding (%)	2.2	1.7	2.8	2.2	1.5
Unfolding prior steepness (%)	1.4–4.8	0.5–4.0	2.9–8.0	0.9–4.4	1.1–1.5
Regularization strength (%)	3.1–3.9	2.3–4.4	3.6–5.8	2.3–5.6	1.1–4.7
Minimum p_T cut-off (%)	1.1–0.3	2.3–0.1	1.3–1.4	2.8–4.1	1.2–0.4
Background estimate (%)	1.8–0.6	3.7–1.5	1.8–0.6	3.7–1.5	2.0–0.9
$\delta p_{T,\text{ch}}$ estimate (%)	0.0–0.0	0.1–0.0	0.0–0.0	0.1–0.0	0.1–0.0
Combined uncertainty (%)	9.2–14.4	11.5–15.5	7.1–11.9	7.5–10.7	3.8–5.7
(T_{pPb}) (%)	–	–	3.4	3.4	–
pp cross section (%)	–	–	3.5	3.5	–
Reference scaling pp 7 TeV (%)	–	–	10.0	10.0	–
NSD selection efficiency p–Pb (%)	–	–	3.1	3.1	–
Combined scaling uncertainty (%)	–	–	11.6	11.6	–

selection criteria and jet finding algorithm can be used on final state particle level, as in the analysis of the real data, in particular, the limitation to charged constituents of a jet. The dominant uncertainty in the parton level calculation is given by the choice of renormalization scale, μ_R , and factorization scale, μ_F . The default value has been chosen to be $\mu_R = \mu_F = p_T$ and independent variations by a factor of two around the central value are considered as the systematic uncertainty. In addition, the uncertainty on the parton distribution functions has been taken into account by the variation of the final results for the respective error sets of the parton density functions (PDFs).

For the comparison with the measured p–Pb data, proton PDFs corrected for nuclear effects (CTEQ6.6 [58] with EPS09 [59]) have been used. Prior to passing the scattered partons to PYTHIA8 for showering, they can be boosted into the same reference frame as the p–Pb reaction by $y_{\text{NN}} = 0.465$.

The construction of the pp reference at $\sqrt{s_{\text{NN}}} = 5.02$ TeV is based on the ALICE measurement of charged jets in pp collisions at 7 TeV, described in detail in [54]. For the purpose of the reference scaling, the same analysis chain has been used as for p–Pb. The same binning in pseudorapidity and transverse momentum allows for a partial cancellation of common systematic uncertainties in the pp and p–Pb data sets. In addition, the same background subtraction approach as in the p–Pb analysis is used for the pp data. In the present analysis, the scaling is done with a factor which is determined for each $p_{T,\text{ch jet}}$ bin by the NLO pQCD calculations (POWHEG + PYTHIA8) at the two energies. For the pp reference scaling the parton distribution functions in the POWHEG calculation have been replaced by the free proton PDF from CTEQ6.6. The scaling factor is given by

$$F(p_T) = \frac{\text{yield}(p_{T,\text{ch jet}})|_{\text{pp, NLO}}^{5.02 \text{ TeV, boosted}}}{\text{yield}(p_{T,\text{ch jet}})|_{\text{pp, NLO}}^{7 \text{ TeV}}} \quad (6)$$

The factor decreases monotonically from $F \approx 0.65$ to 0.45 in the reported p_T range. As already described above, the laboratory frame is not the center-of-mass frame of the collision as is the case for pp collisions. Therefore, the numerator of the scaling factor F in Eq. (6) is determined in the NLO calculation where the additional Lorentz-boost is applied to the hard scattered partons prior to fragmentation. The resulting reduction of the observed jets for $|\eta_{\text{lab}}| < 0.5$ is smaller than 5% in the relevant momentum range.

2.6. Jet production cross section ratio

The broadening or narrowing of the parton shower with respect to the original parton direction can have a direct impact on the jet production cross section reconstructed with different resolution parameters. This can be tested via the ratio of yields or cross sections in common rapidity interval, here $|\eta_{\text{lab}}| < 0.5$ for $R = 0.2$ and 0.4:

$$\mathcal{R}(0.2, 0.4) = \frac{d\sigma_{\text{pPb}, R=0.2}/dp_T}{d\sigma_{\text{pPb}, R=0.4}/dp_T} \quad (7)$$

Considering the extreme scenario that all fragments are already contained within $R = 0.2$ this ratio is unity. In this case, also the statistical uncertainties between $R = 0.2$ and $R = 0.4$ are fully correlated and cancel completely in the ratio, when the jets are reconstructed from the same data set. In the case the jets are less collimated, the ratio decreases and the statistical uncertainties only cancel partially. For the analysis presented in this paper, the conditional probability for reconstructing an $R = 0.2$ jet in the same p_T -bin as a geometrically close $R = 0.4$ jet is 25–50%, which leads to a reduction of the statistical uncertainty of the ratio of 5–10% compared to the case of no correlation.

2.7. Systematic uncertainties

The various sources of systematic uncertainties are listed in Table 2 for the full p_T -range of the three observables presented in this paper: jet production cross section, nuclear modification factor, and cross section ratio. The most important sources will be discussed in the following.

The dominant source of uncertainty for the p_T -differential jet production cross section is the imperfect knowledge of the single-particle tracking efficiency that has a direct impact on the correction of the jet momentum in the unfolding, as discussed above. In p–Pb collisions, the single-particle efficiency is known with a relative accuracy of 4%, which is equivalent to a 4% uncertainty on the jet momentum scale. To estimate the effect of the tracking efficiency uncertainty on the jet yield, the tracking efficiency is artificially lowered by randomly discarding a certain fraction (4% in p–Pb) of tracks used as input for the jet finding. Depending on the shape of the spectrum, the uncertainty on the single particle efficiency (jet momentum scale) translates into an uncertainty of 8 to 15% on the yield.

To estimate the uncertainty on the p–Pb nuclear modification factor, the uncertainty on the single-particle tracking efficiency

in the two collision systems (pp and p–Pb) has to be evaluated. This uncertainty on the efficiency is correlated between the data sets, since the correction is determined with the same underlying Monte Carlo description of the ALICE detector and for similar track quality cuts. Only variations of detector conditions between run periods may reduce the degree of correlation. The uncorrelated uncertainty has been estimated to be 2%, and the uncertainty for the nuclear modification factor has been determined by artificially introducing such a difference in the tracking efficiency between the two collision systems.

The uncertainty on the spectra induced by the underlying event subtraction has been estimated by comparing the results with various methods for background subtraction; ranging from purely track-based to jet-based density estimates, including an η_{lab} -dependent correction. As seen in Fig. 1, a typical correction $\pi R^2 \rho_{\text{ch}}$ for a jet with $R = 0.4$ is about 1 GeV/c. The uncertainty on this correction can be treated similar to an uncertainty on the jet momentum scale. For the final spectrum, the uncertainty on the yields from the background correction method is approximately 2%.

In the determination of the fluctuations of the underlying event, the main uncertainty is given by the exclusion of reconstructed jets in the random cone sampling of the event. The probability for a random cone to overlap with reconstructed jets is higher than for the jets itself. On average, a jet can overlap with $N_{\text{coll}} - 1$ jets in one event. The random cone can overlap with N_{coll} jets. To account for this, the $\delta p_{T,\text{ch}}$ calculation can be modified to discard on a statistical basis random cones that overlap with signal jets. This lowers the average overlap probability. However, since this modified $\delta p_{T,\text{ch}}$ calculation strongly depends on the signal jet definition and also on how an overlap is defined, it is not used by default but considered for systematic uncertainties. The effect of this partial signal exclusion approach on the fully corrected jet yields is of the order of 0.1%.

The uncertainty of the scaling procedure to obtain the reference spectrum is estimated by determining the scaling factors $F(p_T)$ after varying the scales μ_R and μ_F in the POWHEG NLO generation, and by using different tunes in the outgoing fragmentation handled by PYTHIA8. Furthermore, standalone calculations with PYTHIA6 and PYTHIA8 using different generator tunes and with HERWIG at the two energies have been performed to obtain scaling factors according to Eq. (6). A general uncertainty for how well LO generators and NLO calculations can describe the \sqrt{s} -dependence of particle production is also considered: in ALICE measurements of the π^0 production in pp collisions, it has been observed that pQCD calculations predict a stronger increase of the production cross section when going from 0.9 to 7 TeV than supported by the data [60]. A similar effect is also seen in unidentified charged hadrons measured with ALICE at 0.9, 2.76, and 7 TeV [61]. Furthermore, the \sqrt{s} -dependence of the jet production cross section has been cross checked internally with an interpolation between 7 and 2.76 TeV, using preliminary ALICE results on charged jets at $\sqrt{s} = 2.76$ TeV. In total, these studies yield an additional uncertainty on the pp reference of 10% for the extrapolation from 7 to 5.02 TeV. It is reported as an independent normalization uncertainty, similar to the uncertainty on the nuclear overlap function.

3. Results

The p_T -differential production cross sections for jets reconstructed from charged particles in minimum bias p–Pb collisions at $\sqrt{s_{\text{NN}}} = 5.02$ TeV are shown in Figs. 3 and 4 for the resolution parameters $R = 0.4$ and $R = 0.2$. The spectra are found to agree well with scaled NLO pQCD calculations (POWHEG + PYTHIA8) using nuclear PDFs (CTEQ6.6 + EPS09) as seen best in the ratio data

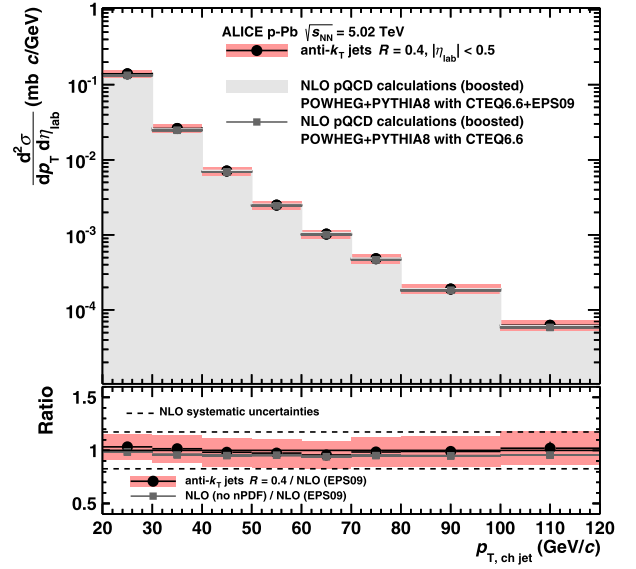


Fig. 3. (Color online.) Top panel: p_T -differential production cross section of charged jet production in p–Pb collisions at 5.02 TeV for $R = 0.4$. Bottom panel: Ratio of data and NLO pQCD calculations. The global uncertainty from the measurement of the visible cross section of 3.5% is not shown. The uncertainties on the pQCD calculation are only shown in the ratio plot as dashed lines. The pQCD calculations take into account the rapidity shift of the nucleon–nucleon center-of-mass system in p–Pb with a boosted parton system.

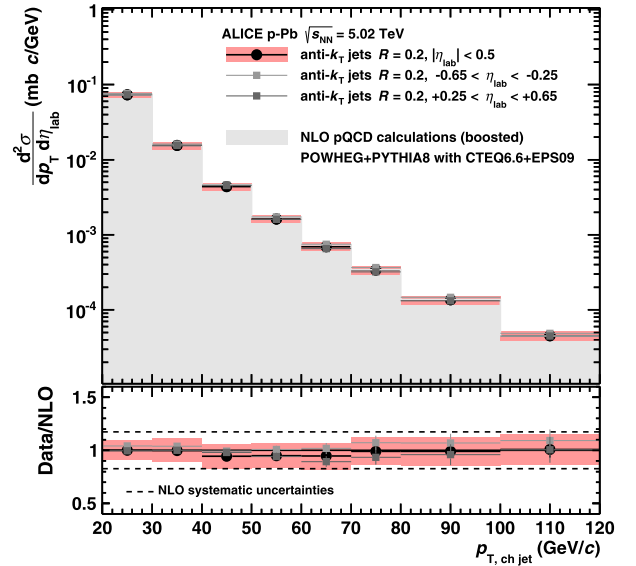


Fig. 4. (Color online.) Top panel: p_T -differential production cross section of charged jet production in p–Pb collisions at 5.02 TeV for $R = 0.2$. Bottom panel: Ratio of data and NLO pQCD calculations. The global uncertainty from the measurement of the visible cross section of 3.5% is not shown. The uncertainties on the pQCD calculation are only shown in the ratio plot as dashed lines. The pQCD calculations take into account the rapidity shift of the nucleon–nucleon center-of-mass system in p–Pb with a boosted parton system.

over calculation in the lower panels. However, the effect of the nuclear PDFs on the jet production in the reported kinematic regime is almost negligible, as seen in the comparison to calculations with only proton PDFs (CTEQ6.6).

Fig. 4 also shows the jet spectra for $-0.65 < \eta_{\text{lab}} < -0.25$ and $0.25 < \eta_{\text{lab}} < 0.65$ compared to the results from the symmetric selection $|\eta_{\text{lab}}| < 0.5$. Here, η_{lab} denotes the pseudorapidity of the jet axis. The first selection roughly corresponds to a small window around mid-rapidity for the nucleon–nucleon center-of-mass

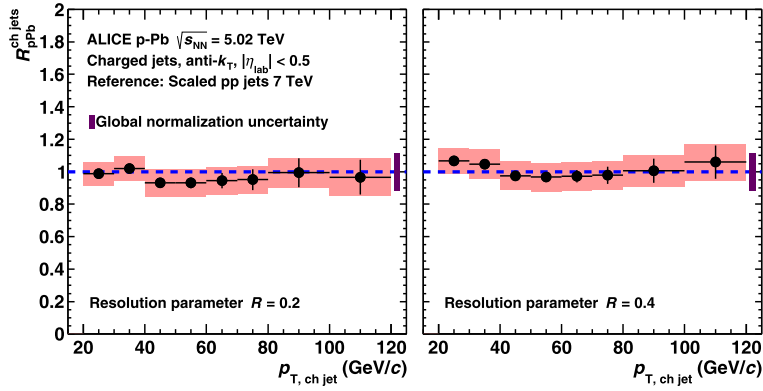


Fig. 5. (Color online.) Nuclear modification factors R_{pPb} of charged jets for $R = 0.2$ (left) and $R = 0.4$ (right). The combined global normalization uncertainty from $\langle T_{pPb} \rangle$, the correction to NSD events, the measured pp cross section, and the reference scaling is depicted by the box around unity.

system, while the second is separated from it by about one unit in rapidity. No significant change of the jet spectra is observed for these two η_{lab} regions centered at -0.45 and 0.45 . Thus, the jet measurement has no strong sensitivity to the rapidity shift and the pseudorapidity dependent variation of the multiplicity (underlying event) within the statistical and systematic uncertainties of the measurement.

The nuclear modification factor R_{pPb} is constructed based on the p_T -differential yields and the extrapolated pp production cross section at 5.02 TeV for $R = 0.2$ and 0.4 . It is shown in the left and right panel of Fig. 5, respectively. In the reported p_T -range, it is consistent with unity, indicating the absence of a large modification of the initial parton distributions or a strong final state effect on jet production. Before comparing these results to the measured single-particle results for R_{pPb} , one has to consider that the same reconstructed p_T corresponds to a different underlying parton transverse momentum. Assuming that all spectra should obey the same power law behavior at high p_T , an effective conversion between the spectra can be derived at a given energy via the POWHEG+PYTHIA8 simulations described above. To match the single charged particle spectra in the simulation to charged jets with $R = 0.4$, a transformation $p_T^{h^\pm} \rightarrow 2.28 p_T^{h^\pm}$ is needed. Thus, the reported nuclear modification factor for charged jets probes roughly the same parton p_T -region as the ALICE measurement of single charged particles that shows a nuclear modification factor in agreement with unity in the measured high- p_T range up to 50 GeV/c [27].

Since the jet measurements integrate the final state particles, they have a smaller sensitivity to the fragmentation pattern of partons than single particles. Differences between the nuclear modification factor for jets and single high- p_T particles, as suggested by measurements in [28,29], could point to a modified fragmentation pattern or differently biased jet selection in p–Pb collisions.

A modified fragmentation pattern may be also reflected in the collimation or transverse structure of jets. The first step in testing possible cold nuclear matter effects on the jet structure is the ratio of jet production cross sections for two different resolution parameters. It is shown for $R = 0.2$ and $R = 0.4$ in p–Pb in Fig. 6 and compared to PYTHIA6 (Tune Perugia 2011) and POWHEG+PYTHIA8 at $\sqrt{s_{NN}} = 5.02$ TeV and to ALICE results in pp collisions at $\sqrt{s} = 7$ TeV [54]. All data show the expected increase of the ratio from the increasing collimation of jets for higher transverse momentum and agree well within the uncertainties. No significant energy dependence or change with collision species is observed. The data for p–Pb collisions is well described by the NLO calculation as well as by the simulation of pp collisions with PYTHIA6 at the same energy. It should be noted that the ratio for

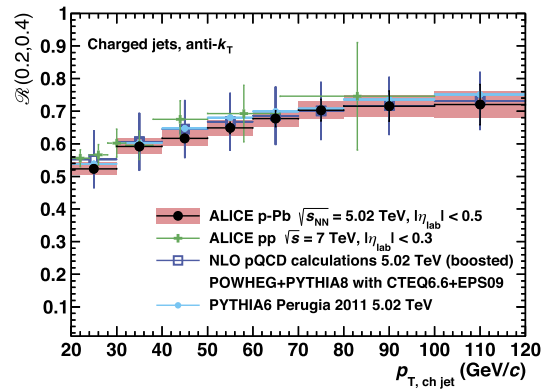


Fig. 6. (Color online.) Charged jet production cross section ratio for different resolution parameters as defined in Eq. (7). The data in p–Pb collisions at $\sqrt{s_{NN}} = 5.02$ TeV are compared to PYTHIA6 (tune: Perugia 2011, no uncertainties shown) and POWHEG+PYTHIA8 (combined stat. and syst. uncertainties shown) at the same energy, and to pp collisions at 7 TeV (only stat. uncertainties shown).

charged jets is, in general, above the ratio obtained for fully reconstructed jets, containing charged and neutral constituents. This can be understood from the contribution from neutral pions that decay already at the collision vertex and lead to an effective broadening of the jet profile when including the neutral component in the jet reconstruction, mainly in the form of decay photons. For the same reason, the inclusion of the hadronization in the NLO pQCD calculation is essential to describe the ratio of jet production cross section as also discussed in [62].

4. Summary

In this paper, p_T -differential charged jet production cross sections in p–Pb collisions at $\sqrt{s_{NN}} = 5.02$ TeV have been shown up to $p_{T, ch,jet}$ of 120 GeV/c for resolution parameters $R = 0.2$ and $R = 0.4$. The charged jet production is found to be compatible with scaled pQCD calculations at the same energy using nuclear PDFs. At the same time, the nuclear modification factor R_{pPb} (using a scaled measurement of jets in pp collisions at $\sqrt{s} = 7$ TeV as a reference) does not show strong nuclear effects on jet production and is consistent with unity for $R = 0.4$ and $R = 0.2$ in the measured p_T -range between 20 and 120 GeV/c. The jet cross section ratio of $R = 0.2/0.4$ is compatible with 7 TeV pp data and also with the predictions from PYTHIA6 Perugia 2011 and POWHEG+PYTHIA8 calculations at 5.02 TeV. No indication of a strong nuclear modification of the jet radial profile is observed, comparing jets with different resolution parameters $R = 0.2$ and $R = 0.4$.

Acknowledgements

The ALICE Collaboration would like to thank all its engineers and technicians for their invaluable contributions to the construction of the experiment and the CERN accelerator teams for the outstanding performance of the LHC complex. The ALICE Collaboration gratefully acknowledges the resources and support provided by all Grid centres and the Worldwide LHC Computing Grid (WLCG) Collaboration. The ALICE Collaboration acknowledges the following funding agencies for their support in building and running the ALICE detector: State Committee of Science, World Federation of Scientists (WFS) and Swiss Fonds Kidagan, Armenia, Conselho Nacional de Desenvolvimento Científico e Tecnológico (CNPq), Financiadora de Estudos e Projetos (FINEP), Fundação de Amparo à Pesquisa do Estado de São Paulo (FAPESP); National Natural Science Foundation of China (NSFC), the Chinese Ministry of Education (CMOE) and the Ministry of Science and Technology of the People's Republic of China (MSTC); Ministry of Education and Youth of the Czech Republic; Danish Natural Science Research Council, the Carlsberg Foundation and the Danish National Research Foundation; The European Research Council under the European Community's Seventh Framework Programme; Helsinki Institute of Physics and the Academy of Finland; French CNRS-IN2P3, the 'Region Pays de Loire', 'Region Alsace', 'Region Auvergne' and CEA, France; German Bundesministerium für Bildung, Wissenschaft, Forschung und Technologie (BMBF) and the Helmholtz Association; General Secretariat for Research and Technology, Ministry of Development, Greece; Hungarian Országos Tudományos Kutatási Alapprogramok (OTKA) and National Office for Research and Technology (NKTH); Department of Atomic Energy and Department of Science and Technology of the Government of India; Istituto Nazionale di Fisica Nucleare (INFN) and Centro Fermi – Museo Storico della Fisica e Centro Studi e Ricerche "Enrico Fermi", Italy; MEXT Grant-in-Aid for Specially Promoted Research, Japan; Joint Institute for Nuclear Research, Dubna; National Research Foundation of Korea (NRF); Consejo Nacional de Ciencia y Tecnología (CONACYT), Dirección General de Asuntos del Personal Académico (DGAPA), México; Amérique Latine Formation académique–European Commission (ALFA–EC) and the EPLANET Program (European Particle Physics Latin American Network); Stichting voor Fundamenteel Onderzoek der Materie (FOM) and the Nederlandse Organisatie voor Wetenschappelijk Onderzoek (NWO), Netherlands; Research Council of Norway (NFR); National Science Centre of Poland; Ministry of National Education/Institute for Atomic Physics and Consiliul Național al Cercetării Științifice–Executive Agency for Higher Education Research Development and Innovation Funding (CNCS–UEFISCDI) – Romania; Ministry of Education and Science of the Russian Federation, Russian Academy of Sciences, Russian Federal Agency of Atomic Energy, Russian Federal Agency for Science and Innovations and The Russian Foundation for Basic Research; Ministry of Education of Slovakia; Department of Science and Technology, Republic of South Africa; Centro de Investigaciones Energéticas, Medioambientales y Tecnológicas (CIEMAT), E-Infrastructure shared between Europe and Latin America (EELA), Ministerio de Economía y Competitividad (MINECO) of Spain, Xunta de Galicia (Consellería de Educación), Centro de Aplicaciones Tecnológicas y Desarrollo Nuclear (CEADEN), Cubaenergía, Cuba, and IAEA (International Atomic Energy Agency); Swedish Research Council (VR) and Knut & Alice Wallenberg Foundation (KAW); Ukraine Ministry of Education and Science; United Kingdom Science and Technology Facilities Council (STFC); The United States Department of Energy, the United States National Science Foundation, the State of Texas, and the State of Ohio; Ministry of Science, Education and Sports of Croatia and Unity through Knowledge Fund, Croatia; Council of Scientific and Industrial Research (CSIR), New Delhi, India.

References

- [1] J.C. Collins, et al., Factorization for short distance hadron–hadron scattering, *Nucl. Phys. B* 261 (1985) 104.
- [2] L.D. McLerran, The color glass condensate and small x physics: four lectures, *Lect. Notes Phys.* 583 (2002) 291–334, arXiv:hep-ph/0104285.
- [3] C. Salgado, et al., Proton–nucleus collisions at the LHC: scientific opportunities and requirements, *J. Phys. G* 39 (2012) 015010, arXiv:1105.3919 [hep-ph].
- [4] A. Krzywicki, J. Engels, B. Petersson, U. Sukhatme, Does a nucleus act like a gluon filter?, *Phys. Lett. B* 85 (1979) 407.
- [5] A. Accardi, Final state interactions and hadron quenching in cold nuclear matter, *Phys. Rev. C* 76 (2007) 034902, arXiv:0706.3227 [nucl-th].
- [6] ALICE Collaboration, K. Aamodt, et al., Suppression of charged particle production at large transverse momentum in central Pb–Pb collisions at $\sqrt{s_{NN}} = 2.76$ TeV, *Phys. Lett. B* 696 (2011) 30–39, arXiv:1012.1004 [nucl-ex].
- [7] ALICE Collaboration, K. Aamodt, et al., Particle–yield modification in jet-like azimuthal di-hadron correlations in Pb–Pb collisions at $\sqrt{s_{NN}} = 2.76$ TeV, *Phys. Rev. Lett.* 108 (2012) 092301, arXiv:1110.0121 [nucl-ex].
- [8] CMS Collaboration, S. Chatrchyan, et al., Study of high- p_T charged particle suppression in PbPb compared to pp collisions at $\sqrt{s_{NN}} = 2.76$ TeV, *Eur. Phys. J. C* 72 (2012) 1945, arXiv:1202.2554 [nucl-ex].
- [9] ATLAS Collaboration, G. Aad, et al., Observation of a centrality-dependent dijet asymmetry in lead–lead collisions at $\sqrt{s_{NN}} = 2.76$ TeV with the ATLAS detector at the LHC, *Phys. Rev. Lett.* 105 (2010) 252303, arXiv:1011.6182 [hep-ex].
- [10] CMS Collaboration, S. Chatrchyan, et al., Jet momentum dependence of jet quenching in PbPb collisions at $\sqrt{s_{NN}} = 2.76$ TeV, *Phys. Lett. B* 712 (2012) 176–197, arXiv:1202.5022 [nucl-ex].
- [11] ATLAS Collaboration, G. Aad, et al., Measurement of the jet radius and transverse momentum dependence of inclusive jet suppression in lead–lead collisions at $\sqrt{s_{NN}} = 2.76$ TeV with the ATLAS detector, *Phys. Lett. B* 719 (2013) 220–241, arXiv:1208.1967 [hep-ex].
- [12] ALICE Collaboration, B. Abelev, et al., Measurement of charged jet suppression in Pb–Pb collisions at $\sqrt{s_{NN}} = 2.76$ TeV, *J. High Energy Phys.* 1403 (2014) 013, arXiv:1311.0633 [nucl-ex].
- [13] ATLAS Collaboration, G. Aad, et al., Measurements of the nuclear modification factor for jets in Pb + Pb collisions at $\sqrt{s_{NN}} = 2.76$ TeV with the ATLAS detector, arXiv:1411.2357 [hep-ex].
- [14] PHENIX Collaboration, K. Adcox, et al., Suppression of hadrons with large transverse momentum in central Au + Au collisions at $\sqrt{s_{NN}} = 130$ GeV, *Phys. Rev. Lett.* 88 (2002) 022301, arXiv:nucl-ex/0109003.
- [15] PHENIX Collaboration, S.S. Adler, et al., Suppressed π^0 production at large transverse momentum in central Au + Au collisions at $\sqrt{s_{NN}} = 200$ GeV, *Phys. Rev. Lett.* 91 (2003) 072301, arXiv:nucl-ex/0304022.
- [16] STAR Collaboration, J. Adams, et al., Transverse momentum and collision energy dependence of high p_T hadron suppression in Au + Au collisions at ultrarelativistic energies, *Phys. Rev. Lett.* 91 (2003) 172302, arXiv:nucl-ex/0305015.
- [17] STAR Collaboration, J. Adams, et al., Evidence from d + Au measurements for final-state suppression of high p_T hadrons in Au + Au collisions at RHIC, *Phys. Rev. Lett.* 91 (2003) 072304, arXiv:nucl-ex/0306024.
- [18] BRAHMS Collaboration, I. Arsene, et al., Transverse momentum spectra in Au + Au and d + Au collisions at $\sqrt{s} = 200$ GeV and the pseudorapidity dependence of high p_T suppression, *Phys. Rev. Lett.* 91 (2003) 072305, arXiv:nucl-ex/0307003.
- [19] PHOBOS Collaboration, B.B. Back, et al., Charged hadron transverse momentum distributions in Au + Au collisions at $\sqrt{s_{NN}} = 200$ GeV, *Phys. Lett. B* 578 (2004) 297–303, arXiv:nucl-ex/0302015.
- [20] M. Gyulassy, M. Plumer, Jet quenching in dense matter, *Phys. Lett. B* 243 (1990) 432–438.
- [21] R. Baier, et al., Induced gluon radiation in a qcd medium, *Phys. Lett. B* 345 (1995) 277–286, arXiv:hep-ph/9411409.
- [22] CMS Collaboration, S. Chatrchyan, et al., Observation of long-range near-side angular correlations in proton–lead collisions at the LHC, *Phys. Lett. B* 718 (2013) 795–814, arXiv:1210.5482 [nucl-ex].
- [23] ALICE Collaboration, B. Abelev, et al., Long-range angular correlations on the near and away side in p–Pb collisions at $\sqrt{s_{NN}} = 5.02$ TeV, *Phys. Lett. B* 719 (2013) 29–41, arXiv:1212.2001 [nucl-ex].
- [24] ATLAS Collaboration, G. Aad, et al., Measurement with the ATLAS detector of multi-particle azimuthal correlations in p + Pb collisions at $\sqrt{s_{NN}} = 5.02$ TeV, *Phys. Lett. B* 725 (2013) 60–78, arXiv:1303.2084 [hep-ex].
- [25] ALICE Collaboration, B.B. Abelev, et al., Long-range angular correlations of pi, K and p in p–Pb collisions at $\sqrt{s_{NN}} = 5.02$ TeV, *Phys. Lett. B* 726 (2013) 164–177, arXiv:1307.3237 [nucl-ex].
- [26] ALICE Collaboration, B. Abelev, et al., Transverse momentum distribution and nuclear modification factor of charged particles in p–Pb collisions at $\sqrt{s_{NN}} = 5.02$ TeV, *Phys. Rev. Lett.* 110 (2013) 082302, arXiv:1210.4520 [nucl-ex].
- [27] ALICE Collaboration, B.B. Abelev, et al., Transverse momentum dependence of inclusive primary charged-particle production in p–Pb collisions at $\sqrt{s_{NN}} = 5.02$ TeV, *Eur. Phys. J. C* 74 (2014) 3054, arXiv:1405.2737 [nucl-ex].

- [28] CMS Collaboration, V. Khachatryan, et al., Nuclear effects on the transverse momentum spectra of charged particles in pPb collisions at a nucleon–nucleon center-of-mass energy of 5.02 TeV, arXiv:1502.05387 [nucl-ex].
- [29] ATLAS Collaboration, Charged hadron production in p+Pb collisions at $\sqrt{s_{NN}} = 5.02$ TeV measured at high transverse momentum by the ATLAS experiment, <http://cds.cern.ch/record/1704978>.
- [30] ATLAS Collaboration, G. Aad, et al., Centrality and rapidity dependence of inclusive jet production in $\sqrt{s_{NN}} = 5.02$ TeV proton–lead collisions with the ATLAS detector, arXiv:1412.4092 [hep-ex].
- [31] CMS Collaboration, S. Chatrchyan, et al., Studies of dijet transverse momentum balance and pseudorapidity distributions in pPb collisions at $\sqrt{s_{NN}} = 5.02$ TeV, Eur. Phys. J. C 74 (7) (2014) 2951, arXiv:1401.4433 [nucl-ex].
- [32] J.E. Huth, et al., Toward a standardization of jet definitions, in: Summer Study on High Energy Physics, Research Directions for the Decade, Snowmass, CO, Jun 25–Jul 13, 1990.
- [33] M. Cacciari, G.P. Salam, Dispelling the N^3 myth for the k_t jet-finder, Phys. Lett. B 641 (2006) 57–61, arXiv:hep-ph/0512210.
- [34] M. Cacciari, et al., Fluctuations and asymmetric jet events in PbPb collisions at the LHC, Eur. Phys. J. C 71 (2011) 1692, arXiv:1101.2878 [hep-ph].
- [35] ALICE Collaboration, B. Abelev, et al., Measurement of event background fluctuations for charged particle jet reconstruction in Pb–Pb collisions at $\sqrt{s_{NN}} = 2.76$ TeV, J. High Energy Phys. 1203 (2012) 053, arXiv:1201.2423 [hep-ex].
- [36] ALICE Collaboration, B. Abelev, et al., Performance of the ALICE experiment at the CERN LHC, Int. J. Mod. Phys. A 29 (24) (2014) 1430044, arXiv:1402.4476 [nucl-ex].
- [37] ALICE Collaboration, K. Aamodt, et al., Charged-particle multiplicity density at mid-rapidity in central Pb–Pb collisions at $\sqrt{s_{NN}} = 2.76$ TeV, Phys. Rev. Lett. 105 (25) (December 2010) 252301, arXiv:1011.3916 [nucl-ex].
- [38] ALICE Collaboration, J. Adam, et al., Centrality dependence of particle production in p–Pb collisions at $\sqrt{s_{NN}} = 5.02$ TeV, arXiv:1412.6828 [nucl-ex].
- [39] ALICE Collaboration, B.B. Abelev, et al., Measurement of visible cross sections in proton–lead collisions at $\sqrt{s_{NN}} = 5.02$ TeV in van der Meer scans with the ALICE detector, J. Instrum. 9 (11) (2014) P11003, arXiv:1405.1849 [nucl-ex].
- [40] ALICE Collaboration, B. Abelev, et al., Pseudorapidity density of charged particles p–Pb collisions at $\sqrt{s_{NN}} = 5.02$ TeV, Phys. Rev. Lett. 110 (2013) 032301, arXiv:1210.3615 [nucl-ex].
- [41] ALICE Collaboration, K. Aamodt, et al., Alignment of the ALICE inner tracking system with cosmic-ray tracks, J. Instrum. 5 (2010) P03003, arXiv:1001.0502 [physics.ins-det].
- [42] J. Alme, et al., The ALICE TPC, a large 3-dimensional tracking device with fast readout for ultra-high multiplicity events, Nucl. Instrum. Methods Phys. Res., Sect. A, Accel. Spectrom. Detect. Assoc. Equip. 622 (2010) 316–367, arXiv:1001.1950 [physics.ins-det].
- [43] M. Cacciari, et al., The anti- k_t jet clustering algorithm, J. High Energy Phys. 0804 (2008) 063, arXiv:0802.1189 [hep-ph].
- [44] M. Cacciari, G.P. Salam, G. Soyez, The catchment area of jets, J. High Energy Phys. 04 (2008) 005, arXiv:0802.1188 [hep-ph].
- [45] CMS Collaboration, S. Chatrchyan, et al., Measurement of the underlying event activity in pp collisions at $\sqrt{s} = 0.9$ and 7 TeV with the novel jet-area/median approach, J. High Energy Phys. 1208 (2012) 130, arXiv:1207.2392 [hep-ex].
- [46] ALICE Collaboration, B. Abelev, et al., Underlying event measurements in pp collisions at $\sqrt{s} = 0.9$ and 7 TeV with the ALICE experiment at the LHC, J. High Energy Phys. 1207 (2012) 116, arXiv:1112.2082 [hep-ex].
- [47] T. Sjöstrand, et al., PYTHIA 6.4 physics and manual, J. High Energy Phys. 05 (2006) 026, arXiv:hep-ph/0603175.
- [48] R. Brun, F. Carminati, GEANT, Detector Description and Simulation Tool, CERN Program Library Long Writeup W5013, 1993.
- [49] A. Hocker, V. Kartvelishvili, SVD approach to data unfolding, Nucl. Instrum. Methods Phys. Res., Sect. A, Accel. Spectrom. Detect. Assoc. Equip. 372 (1996) 469–481, arXiv:hep-ph/9509307.
- [50] T. Adye, Unfolding algorithms and tests using RooUnfold, arXiv:1105.1160 [physics.data-an].
- [51] V. Blobel, An unfolding method for high-energy physics experiments, arXiv:hep-ex/0208022.
- [52] G. D’Agostini, Bayesian inference in processing experimental data principles and basic applications, arXiv:physics/0304102.
- [53] V. Blobel, in: 8th CERN School of Computing, CSC '84, Aiguablava, Spain, 9–22 Sep., 1984.
- [54] ALICE Collaboration, B. Abelev, Charged jet cross sections and properties in proton–proton collisions at $\sqrt{s} = 7$ TeV, arXiv:1411.4969 [nucl-ex].
- [55] P. Nason, A new method for combining NLO QCD with shower Monte Carlo algorithms, J. High Energy Phys. 0411 (2004) 040, arXiv:hep-ph/0409146.
- [56] S. Frixione, P. Nason, G. Ridolfi, A positive-weight next-to-leading-order Monte Carlo for heavy flavour hadroproduction, J. High Energy Phys. 0709 (2007) 126, arXiv:0707.3088 [hep-ph].
- [57] T. Sjöstrand, S. Mrenna, P.Z. Skands, A brief introduction to PYTHIA 8.1, Comput. Phys. Commun. 178 (2008) 852–867, arXiv:0710.3820 [hep-ph].
- [58] P.M. Nadolsky, H.-L. Lai, Q.-H. Cao, J. Huston, J. Pumplin, et al., Implications of CTEQ global analysis for collider observables, Phys. Rev. D 78 (2008) 013004, arXiv:0802.0007 [hep-ph].
- [59] K.J. Eskola, H. Paukkunen, C.A. Salgado, EPS09 – a new generation of NLO and LO nuclear parton distribution functions, J. High Energy Phys. 04 (2009) 065, arXiv:0902.4154 [hep-ph].
- [60] ALICE Collaboration, B. Abelev, et al., Neutral pion and η meson production in proton–proton collisions at $\sqrt{s} = 0.9$ TeV and $\sqrt{s} = 7$ TeV, Phys. Lett. B 717 (2012) 162–172, arXiv:1205.5724 [hep-ex].
- [61] ALICE Collaboration, B.B. Abelev, et al., Energy dependence of the transverse momentum distributions of charged particles in pp collisions measured by ALICE, Eur. Phys. J. C 73 (2013) 2662, arXiv:1307.1093 [nucl-ex].
- [62] ALICE Collaboration, B. Abelev, et al., Measurement of the inclusive differential jet cross section in pp collisions at $\sqrt{s} = 2.76$ TeV, Phys. Lett. B 722 (4–5) (2013) 262–272, arXiv:1301.3475 [nucl-ex].

ALICE Collaboration

J. Adam³⁹, D. Adamová⁸², M.M. Aggarwal⁸⁶, G. Aglieri Rinella³⁶, M. Agnello¹¹⁰, N. Agrawal⁴⁷, Z. Ahammed¹³⁰, S.U. Ahn⁶⁷, I. Aimo^{93,110}, S. Aiola¹³⁵, M. Ajaz¹⁶, A. Akhmedov⁵⁷, S.N. Alam¹³⁰, D. Aleksandrov⁹⁹, B. Alessandro¹¹⁰, D. Alexandre¹⁰¹, R. Alfaro Molina⁶³, A. Alici^{104,12}, A. Alkin³, J. Alme³⁷, T. Alt⁴², S. Altinpinar¹⁸, I. Altsybeev¹²⁹, C. Alves Garcia Prado¹¹⁸, C. Andrei⁷⁷, A. Andronic⁹⁶, V. Anguelov⁹², J. Anielski⁵³, T. Antičić⁹⁷, F. Antinori¹⁰⁷, P. Antonioli¹⁰⁴, L. Aphecetche¹¹², H. Appelshäuser⁵², S. Arcelli²⁸, N. Armesto¹⁷, R. Arnaldi¹¹⁰, T. Aronsson¹³⁵, I.C. Arsene²², M. Arslandok⁵², A. Augustinus³⁶, R. Averbeck⁹⁶, M.D. Azmi¹⁹, M. Bach⁴², A. Badalà¹⁰⁶, Y.W. Baek⁴³, S. Bagnasco¹¹⁰, R. Bailhache⁵², R. Bala⁸⁹, A. Baldisseri¹⁵, F. Baltasar Dos Santos Pedrosa³⁶, R.C. Baral⁶⁰, A.M. Barbano¹¹⁰, R. Barbera²⁹, F. Barile³³, G.G. Barnaföldi¹³⁴, L.S. Barnby¹⁰¹, V. Barret⁶⁹, P. Bartalini⁷, J. Bartke¹¹⁵, E. Bartsch⁵², M. Basile²⁸, N. Bastid⁶⁹, S. Basu¹³⁰, B. Bathen⁵³, G. Batigne¹¹², A. Batista Camejo⁶⁹, B. Batyunya⁶⁵, P.C. Batzing²², I.G. Bearden⁷⁹, H. Beck⁵², C. Bedda¹¹⁰, N.K. Behera^{48,47}, I. Belikov⁵⁴, F. Bellini²⁸, H. Bello Martinez², R. Bellwied¹²⁰, R. Belmont¹³³, E. Belmont-Moreno⁶³, V. Belyaev⁷⁵, G. Bencedi¹³⁴, S. Beole²⁷, I. Berceanu⁷⁷, A. Bercuci⁷⁷, Y. Berdnikov⁸⁴, D. Berenyi¹³⁴, R.A. Bertens⁵⁶, D. Berzano^{36,27}, L. Betev³⁶, A. Bhasin⁸⁹, I.R. Bhat⁸⁹, A.K. Bhati⁸⁶, B. Bhattacharjee⁴⁴, J. Bhom¹²⁶, L. Bianchi^{27,120}, N. Bianchi⁷¹, C. Bianchin^{133,56}, J. Bielčik³⁹, J. Bielčíková⁸², A. Bilandžić⁷⁹, S. Biswas⁷⁸, S. Bjelogrić⁵⁶, F. Blanco¹⁰, D. Blau⁹⁹, C. Blume⁵², F. Bock^{73,92}, A. Bogdanov⁷⁵, H. Bøggild⁷⁹, L. Boldizsár¹³⁴, M. Bombara⁴⁰, J. Book⁵², H. Borel¹⁵, A. Borissov⁹⁵, M. Borri⁸¹, F. Bossú⁶⁴, M. Botje⁸⁰, E. Botta²⁷, S. Böttger⁵¹, P. Braun-Munzinger⁹⁶,

M. Bregant¹¹⁸, T. Breitner⁵¹, T.A. Brooker⁵², T.A. Browning⁹⁴, M. Broz³⁹, E.J. Brucken⁴⁵, E. Bruna¹¹⁰,
 G.E. Bruno³³, D. Budnikov⁹⁸, H. Buesching⁵², S. Bufalino^{110,36}, P. Buncic³⁶, O. Busch^{92,126},
 Z. Buthelezi⁶⁴, J.T. Buxton²⁰, D. Caffarri^{36,30}, X. Cai⁷, H. Caines¹³⁵, L. Calero Diaz⁷¹, A. Caliva⁵⁶,
 E. Calvo Villar¹⁰², P. Camerini²⁶, F. Carena³⁶, W. Carena³⁶, J. Castillo Castellanos¹⁵, A.J. Castro¹²³,
 E.A.R. Casula²⁵, C. Cavicchioli³⁶, C. Ceballos Sanchez⁹, J. Cepila³⁹, P. Cerello¹¹⁰, B. Chang¹²¹,
 S. Chapeland³⁶, M. Chartier¹²², J.L. Charvet¹⁵, S. Chattopadhyay¹³⁰, S. Chattopadhyay¹⁰⁰, V. Chelnokov³,
 M. Cherney⁸⁵, C. Cheshkov¹²⁸, B. Cheynis¹²⁸, V. Chibante Barroso³⁶, D.D. Chinellato¹¹⁹, P. Chochula³⁶,
 K. Choi⁹⁵, M. Chojnacki⁷⁹, S. Choudhury¹³⁰, P. Christakoglou⁸⁰, C.H. Christensen⁷⁹, P. Christiansen³⁴,
 T. Chujo¹²⁶, S.U. Chung⁹⁵, Z. Chuhnui⁵⁶, C. Cicalo¹⁰⁵, L. Cifarelli^{12,28}, F. Cindolo¹⁰⁴, J. Cleymans⁸⁸,
 F. Colamaria³³, D. Colella³³, A. Collu²⁵, M. Colocci²⁸, G. Conesa Balbastre⁷⁰, Z. Conesa del Valle⁵⁰,
 M.E. Connors¹³⁵, J.G. Contreras^{39,11}, T.M. Cormier⁸³, Y. Corrales Morales²⁷, I. Cortés Maldonado²,
 P. Cortese³², M.R. Cosentino¹¹⁸, F. Costa³⁶, P. Crochet⁶⁹, R. Cruz Albino¹¹, E. Cuautle⁶², L. Cunqueiro³⁶,
 T. Dahms⁹¹, A. Dainese¹⁰⁷, A. Danu⁶¹, D. Das¹⁰⁰, I. Das^{100,50}, S. Das⁴, A. Dash¹¹⁹, S. Dash⁴⁷, S. De¹¹⁸,
 A. De Caro^{31,12}, G. de Cataldo¹⁰³, J. de Cuveland⁴², A. De Falco²⁵, D. De Gruttola^{12,31}, N. De Marco¹¹⁰,
 S. De Pasquale³¹, A. Deisting^{96,92}, A. Deloff⁷⁶, E. Dénes¹³⁴, G. D’Erasmo³³, D. Di Bari³³, A. Di Mauro³⁶,
 P. Di Nezza⁷¹, M.A. Diaz Corchero¹⁰, T. Dietel⁸⁸, P. Dillenseger⁵², R. Divià³⁶, Ø. Djuvsland¹⁸,
 A. Dobrin^{56,80}, T. Dobrowolski^{76,1}, D. Domenicis Gimenez¹¹⁸, B. Dönigus⁵², O. Dordic²², A.K. Dubey¹³⁰,
 A. Dubla⁵⁶, L. Ducroux¹²⁸, P. Dupieux⁶⁹, R.J. Ehlers¹³⁵, D. Elia¹⁰³, H. Engel⁵¹, B. Erazmus^{112,36},
 F. Erhardt¹²⁷, D. Eschweiler⁴², B. Espagnon⁵⁰, M. Estienne¹¹², S. Esumi¹²⁶, J. Eum⁹⁵, D. Evans¹⁰¹,
 S. Evdokimov¹¹¹, G. Eyyubova³⁹, L. Fabbietti⁹¹, D. Fabris¹⁰⁷, J. Faivre⁷⁰, A. Fantoni⁷¹, M. Fasel⁷³,
 L. Feldkamp⁵³, D. Felea⁶¹, A. Feliciello¹¹⁰, G. Feofilov¹²⁹, J. Ferencei⁸², A. Fernández Téllez²,
 E.G. Ferreira¹⁷, A. Ferretti²⁷, A. Festanti³⁰, J. Figiel¹¹⁵, M.A.S. Figueredo¹²², S. Filchagin⁹⁸,
 D. Finogeev⁵⁵, F.M. Fionda¹⁰³, E.M. Fiore³³, M.G. Fleck⁹², M. Floris³⁶, S. Foertsch⁶⁴, P. Foka⁹⁶,
 S. Fokin⁹⁹, E. Fragiaco¹⁰⁹, A. Francescon^{36,30}, U. Frankenfeld⁹⁶, U. Fuchs³⁶, C. Furget⁷⁰, A. Furs⁵⁵,
 M. Fusco Girard³¹, J.J. Gaardhøje⁷⁹, M. Gagliardi²⁷, A.M. Gago¹⁰², M. Gallio²⁷, D.R. Gangadharan⁷³,
 P. Ganoti⁸⁷, C. Gao⁷, C. Garabatos⁹⁶, E. Garcia-Solis¹³, C. Gargiulo³⁶, P. Gasik⁹¹, M. Germain¹¹²,
 A. Gheata³⁶, M. Gheata^{61,36}, P. Ghosh¹³⁰, S.K. Ghosh⁴, P. Gianotti⁷¹, P. Giubellino³⁶, P. Giubilato³⁰,
 E. Gladysz-Dziadus¹¹⁵, P. Glässel⁹², A. Gomez Ramirez⁵¹, P. González-Zamora¹⁰, S. Gorbunov⁴²,
 L. Görlich¹¹⁵, S. Gotovac¹¹⁴, V. Grabski⁶³, L.K. Graczykowski¹³², A. Grelli⁵⁶, A. Grigoras³⁶, C. Grigoras³⁶,
 V. Grigoriev⁷⁵, A. Grigoryan¹, S. Grigoryan⁶⁵, B. Grinyov³, N. Grion¹⁰⁹, J.F. Grosse-Oetringhaus³⁶,
 J.-Y. Grossiord¹²⁸, R. Grosso³⁶, F. Guber⁵⁵, R. Guernane⁷⁰, B. Guerzoni²⁸, K. Gulbrandsen⁷⁹,
 H. Gulkanyan¹, T. Gunji¹²⁵, A. Gupta⁸⁹, R. Gupta⁸⁹, R. Haake⁵³, Ø. Haaland¹⁸, C. Hadjidakis⁵⁰,
 M. Haiduc⁶¹, H. Hamagaki¹²⁵, G. Hamar¹³⁴, L.D. Hanratty¹⁰¹, A. Hansen⁷⁹, J.W. Harris¹³⁵,
 H. Hartmann⁴², A. Harton¹³, D. Hatzifotiadou¹⁰⁴, S. Hayashi¹²⁵, S.T. Heckel⁵², M. Heide⁵³,
 H. Helstrup³⁷, A. Herghelegiu⁷⁷, G. Herrera Corral¹¹, B.A. Hess³⁵, K.F. Hetland³⁷, T.E. Hilden⁴⁵,
 H. Hillemanns³⁶, B. Hippolyte⁵⁴, P. Hristov³⁶, M. Huang¹⁸, T.J. Humanic²⁰, N. Hussain⁴⁴, T. Hussain¹⁹,
 D. Hutter⁴², D.S. Hwang²¹, R. Ilkaev⁹⁸, I. Ilkiv⁷⁶, M. Inaba¹²⁶, C. Ionita³⁶, M. Ippolitov^{75,99}, M. Irfan¹⁹,
 M. Ivanov⁹⁶, V. Ivanov⁸⁴, V. Izucheev¹¹¹, P.M. Jacobs⁷³, C. Jahnke¹¹⁸, H.J. Jang⁶⁷, M.A. Janik¹³²,
 P.H.S.Y. Jayarathna¹²⁰, C. Jena³⁰, S. Jena¹²⁰, R.T. Jimenez Bustamante⁶², P.G. Jones¹⁰¹, H. Jung⁴³,
 A. Jusko¹⁰¹, P. Kalinak⁵⁸, A. Kalweit³⁶, J. Kamin⁵², J.H. Kang¹³⁶, V. Kaplin⁷⁵, S. Kar¹³⁰,
 A. Karasu Uysal⁶⁸, O. Karavichev⁵⁵, T. Karavicheva⁵⁵, E. Karpechev⁵⁵, U. Keschull⁵¹, R. Keidel¹³⁷,
 D.L.D. Keijndener⁵⁶, M. Keil³⁶, K.H. Khan¹⁶, M.M. Khan¹⁹, P. Khan¹⁰⁰, S.A. Khan¹³⁰, A. Khanzadeev⁸⁴,
 Y. Kharlov¹¹¹, B. Kileng³⁷, B. Kim¹³⁶, D.W. Kim^{43,67}, D.J. Kim¹²¹, H. Kim¹³⁶, J.S. Kim⁴³, M. Kim⁴³,
 M. Kim¹³⁶, S. Kim²¹, T. Kim¹³⁶, S. Kirsch⁴², I. Kisel⁴², S. Kiselev⁵⁷, A. Kisiel¹³², G. Kiss¹³⁴, J.L. Klay⁶,
 C. Klein⁵², J. Klein⁹², C. Klein-Bösing⁵³, A. Kluge³⁶, M.L. Knichel⁹², A.G. Knospe¹¹⁶, T. Kobayashi¹²⁶,
 C. Kobdaj¹¹³, M. Kofarago³⁶, M.K. Köhler⁹⁶, T. Kollegger^{42,96}, A. Kolojvari¹²⁹, V. Kondratiev¹²⁹,
 N. Kondratyeva⁷⁵, E. Kondratyuk¹¹¹, A. Konevskikh⁵⁵, C. Kouzinopoulos³⁶, O. Kovalenko⁷⁶,
 V. Kovalenko¹²⁹, M. Kowalski^{36,115}, S. Kox⁷⁰, G. Koyithatta Meethalevedu⁴⁷, J. Kral¹²¹, I. Králik⁵⁸,
 A. Kravčáková⁴⁰, M. Krelina³⁹, M. Kretz⁴², M. Krivda^{101,58}, F. Krizek⁸², E. Kryshen³⁶, M. Krzewicki^{96,42},
 A.M. Kubera²⁰, V. Kučera⁸², T. Kugathasan³⁶, C. Kuhn⁵⁴, P.G. Kuijer⁸⁰, I. Kulakov⁴², J. Kumar⁴⁷,
 L. Kumar^{78,86}, P. Kurashvili⁷⁶, A. Kurepin⁵⁵, A.B. Kurepin⁵⁵, A. Kuryakin⁹⁸, S. Kuschpil⁸², M.J. Kweon⁴⁹,
 Y. Kwon¹³⁶, S.L. La Pointe¹¹⁰, P. La Rocca²⁹, C. Lagana Fernandes¹¹⁸, I. Lakomov^{36,50}, R. Langoy⁴¹,

C. Lara⁵¹, A. Lardeux¹⁵, A. Lattuca²⁷, E. Laudi³⁶, R. Lea²⁶, L. Leardini⁹², G.R. Lee¹⁰¹, S. Lee¹³⁶, I. Legrand³⁶, R.C. Lemmon⁸¹, V. Lenti¹⁰³, E. Leogrande⁵⁶, I. León Monzón¹¹⁷, M. Leoncino²⁷, P. Lévai¹³⁴, S. Li^{7,69}, X. Li¹⁴, J. Lien⁴¹, R. Lietava¹⁰¹, S. Lindal²², V. Lindenstruth⁴², C. Lippmann⁹⁶, M.A. Lisa²⁰, H.M. Ljunggren³⁴, D.F. Lodato⁵⁶, P.I. Loenne¹⁸, V.R. Loggins¹³³, V. Loginov⁷⁵, C. Loizides⁷³, X. Lopez⁶⁹, E. López Torres⁹, A. Lowe¹³⁴, P. Luettig⁵², M. Lunardon³⁰, G. Luparello^{26,56}, P.H.F.N.D. Luz¹¹⁸, A. Maevskaya⁵⁵, M. Mager³⁶, S. Mahajan⁸⁹, S.M. Mahmood²², A. Maire⁵⁴, R.D. Majka¹³⁵, M. Malaev⁸⁴, I. Maldonado Cervantes⁶², L. Malinina⁶⁵, D. Mal'Kevich⁵⁷, P. Malzacher⁹⁶, A. Mamonov⁹⁸, L. Manceau¹¹⁰, V. Manko⁹⁹, F. Manso⁶⁹, V. Manzari^{103,36}, M. Marchisone²⁷, J. Mareš⁵⁹, G.V. Margagliotti²⁶, A. Margotti¹⁰⁴, J. Margutti⁵⁶, A. Marín⁹⁶, C. Markert¹¹⁶, M. Marquard⁵², N.A. Martin⁹⁶, J. Martin Blanco¹¹², P. Martinengo³⁶, M.I. Martínez², G. Martínez García¹¹², M. Martinez Pedreira³⁶, Y. Martynov³, A. Mas¹¹⁸, S. Masciocchi⁹⁶, M. Maserà²⁷, A. Masoni¹⁰⁵, L. Massacrier¹¹², A. Mastroserio³³, H. Masui¹²⁶, A. Matyja¹¹⁵, C. Mayer¹¹⁵, J. Mazer¹²³, M.A. Mazzoni¹⁰⁸, D. McDonald¹²⁰, F. Meddi²⁴, A. Menchaca-Rocha⁶³, E. Meninno³¹, J. Mercado Pérez⁹², M. Meres³⁸, Y. Miake¹²⁶, M.M. Mieskolainen⁴⁵, K. Mikhaylov^{57,65}, L. Milano³⁶, J. Milosevic^{22,131}, L.M. Minervini^{103,23}, A. Mischke⁵⁶, A.N. Mishra⁴⁸, D. Miśkowiec⁹⁶, J. Mitra¹³⁰, C.M. Mitu⁶¹, N. Mohammadi⁵⁶, B. Mohanty^{130,78}, L. Molnar⁵⁴, L. Montaño Zetina¹¹, E. Montes¹⁰, M. Morando³⁰, D.A. Moreira De Godoy¹¹², S. Moretto³⁰, A. Morreale¹¹², A. Morsch³⁶, V. Muccifora⁷¹, E. Mudnic¹¹⁴, D. Mühlheim⁵³, S. Muhuri¹³⁰, M. Mukherjee¹³⁰, H. Müller³⁶, J.D. Mulligan¹³⁵, M.G. Munhoz¹¹⁸, S. Murray⁶⁴, L. Musa³⁶, J. Musinsky⁵⁸, B.K. Nandi⁴⁷, R. Nania¹⁰⁴, E. Nappi¹⁰³, M.U. Naru¹⁶, C. Nattrass¹²³, K. Nayak⁷⁸, T.K. Nayak¹³⁰, S. Nazarenko⁹⁸, A. Nedosekin⁵⁷, L. Nellen⁶², F. Ng¹²⁰, M. Nicassio⁹⁶, M. Niculescu^{61,36}, J. Niedziela³⁶, B.S. Nielsen⁷⁹, S. Nikolaev⁹⁹, S. Nikulin⁹⁹, V. Nikulin⁸⁴, F. Noferini^{104,12}, P. Nomokonov⁶⁵, G. Nooren⁵⁶, J. Norman¹²², A. Nyanin⁹⁹, J. Nystrand¹⁸, H. Oeschler⁹², S. Oh¹³⁵, S.K. Oh⁶⁶, A. Ohlson³⁶, A. Okatan⁶⁸, T. Okubo⁴⁶, L. Olah¹³⁴, J. Oleniacz¹³², A.C. Oliveira Da Silva¹¹⁸, M.H. Oliver¹³⁵, J. Onderwaater⁹⁶, C. Oppedisano¹¹⁰, A. Ortiz Velasquez⁶², A. Oskarsson³⁴, J. Otwinowski^{96,115}, K. Oyama⁹², M. Ozdemir⁵², Y. Pachmayer⁹², P. Pagano³¹, G. Paić⁶², C. Pajares¹⁷, S.K. Pal¹³⁰, J. Pan¹³³, A.K. Pandey⁴⁷, D. Pant⁴⁷, V. Papikyan¹, G.S. Pappalardo¹⁰⁶, P. Pareek⁴⁸, W.J. Park⁹⁶, S. Parmar⁸⁶, A. Passfeld⁵³, V. Paticchio¹⁰³, B. Paul¹⁰⁰, T. Peitzmann⁵⁶, H. Pereira Da Costa¹⁵, E. Pereira De Oliveira Filho¹¹⁸, D. Peresunko^{75,99}, C.E. Pérez Lara⁸⁰, V. Peskov⁵², Y. Pestov⁵, V. Petráček³⁹, V. Petrov¹¹¹, M. Petrovici⁷⁷, C. Petta²⁹, S. Piano¹⁰⁹, M. Pikna³⁸, P. Pillot¹¹², O. Pinazza^{104,36}, L. Pinsky¹²⁰, D.B. Piyarathna¹²⁰, M. Płoskoń⁷³, M. Planinic¹²⁷, J. Pluta¹³², S. Pochybova¹³⁴, P.L.M. Podesta-Lerma¹¹⁷, M.G. Poghosyan⁸⁵, B. Polichtchouk¹¹¹, N. Poljak¹²⁷, W. Poonsawat¹¹³, A. Pop⁷⁷, S. Porteboeuf-Houssais⁶⁹, J. Porter⁷³, J. Pospisil⁸², S.K. Prasad⁴, R. Preghenella^{36,104}, F. Prino¹¹⁰, C.A. Pruneau¹³³, I. Pshenichnov⁵⁵, M. Puccio¹¹⁰, G. Puddu²⁵, P. Pujahari¹³³, V. Punin⁹⁸, J. Putschke¹³³, H. Qvigstad²², A. Rachevski¹⁰⁹, S. Raha⁴, S. Rajput⁸⁹, J. Rak¹²¹, A. Rakotozafindrabe¹⁵, L. Ramello³², R. Raniwala⁹⁰, S. Raniwala⁹⁰, S.S. Räsänen⁴⁵, B.T. Rascanu⁵², D. Rathee⁸⁶, K.F. Read¹²³, J.S. Real⁷⁰, K. Redlich⁷⁶, R.J. Reed¹³³, A. Rehman¹⁸, P. Reichelt⁵², M. Reicher⁵⁶, F. Reidt^{92,36}, X. Ren⁷, R. Renfordt⁵², A.R. Reolon⁷¹, A. Reshetin⁵⁵, F. Rettig⁴², J.-P. Revol¹², K. Reygers⁹², V. Riabov⁸⁴, R.A. Ricci⁷², T. Richert³⁴, M. Richter²², P. Riedler³⁶, W. Riegler³⁶, F. Riggi²⁹, C. Ristea⁶¹, A. Rivetti¹¹⁰, E. Rocco⁵⁶, M. Rodríguez Cahuantzi^{11,2}, A. Rodriguez Manso⁸⁰, K. Røed²², E. Rogochaya⁶⁵, D. Rohr⁴², D. Röhrich¹⁸, R. Romita¹²², F. Ronchetti⁷¹, L. Ronflette¹¹², P. Rosnet⁶⁹, A. Rossi³⁶, F. Roukoutakis⁸⁷, A. Roy⁴⁸, C. Roy⁵⁴, P. Roy¹⁰⁰, A.J. Rubio Montero¹⁰, R. Rui²⁶, R. Russo²⁷, E. Ryabinkin⁹⁹, Y. Ryabov⁸⁴, A. Rybicki¹¹⁵, S. Sadovsky¹¹¹, K. Šafařík³⁶, B. Sahlmüller⁵², P. Sahoo⁴⁸, R. Sahoo⁴⁸, S. Sahoo⁶⁰, P.K. Sahu⁶⁰, J. Saini¹³⁰, S. Sakai⁷¹, M.A. Saleh¹³³, C.A. Salgado¹⁷, J. Salzwedel²⁰, S. Sambyal⁸⁹, V. Samsonov⁸⁴, X. Sanchez Castro⁵⁴, L. Šándor⁵⁸, A. Sandoval⁶³, M. Sano¹²⁶, G. Santagati²⁹, D. Sarkar¹³⁰, E. Scapparone¹⁰⁴, F. Scarlassara³⁰, R.P. Scharenberg⁹⁴, C. Schiaua⁷⁷, R. Schicker⁹², C. Schmidt⁹⁶, H.R. Schmidt³⁵, S. Schuchmann⁵², J. Schukraft³⁶, M. Schulc³⁹, T. Schuster¹³⁵, Y. Schutz^{112,36}, K. Schwarz⁹⁶, K. Schweda⁹⁶, G. Scioli²⁸, E. Scomparin¹¹⁰, R. Scott¹²³, K.S. Seeder¹¹⁸, J.E. Seger⁸⁵, Y. Sekiguchi¹²⁵, I. Selyuzhenkov⁹⁶, K. Senosi⁶⁴, J. Seo^{66,95}, E. Serradilla^{10,63}, A. Sevcenco⁶¹, A. Shabanov⁵⁵, A. Shabetai¹¹², O. Shadura³, R. Shahoyan³⁶, A. Shangaraev¹¹¹, A. Sharma⁸⁹, N. Sharma^{60,123}, K. Shigaki⁴⁶, K. Shtejer^{9,27}, Y. Sibiriyak⁹⁹, S. Siddhanta¹⁰⁵, K.M. Sielewicz³⁶, T. Siemiarczuk⁷⁶, D. Silvermyr^{83,34}, C. Silvestre⁷⁰, G. Simatovic¹²⁷, G. Simonetti³⁶, R. Singaraju¹³⁰, R. Singh⁷⁸, S. Singha^{78,130}, V. Singhal¹³⁰, B.C. Sinha¹³⁰,

T. Sinha¹⁰⁰, B. Sitar³⁸, M. Sitta³², T.B. Skaali²², M. Slupecki¹²¹, N. Smirnov¹³⁵, R.J.M. Snellings⁵⁶, T.W. Snellman¹²¹, C. Søgaard³⁴, R. Soltz⁷⁴, J. Song⁹⁵, M. Song¹³⁶, Z. Song⁷, F. Soramel³⁰, S. Sorensen¹²³, M. Spacek³⁹, E. Spiriti⁷¹, I. Sputowska¹¹⁵, M. Spyropoulou-Stassinaki⁸⁷, B.K. Srivastava⁹⁴, J. Stachel⁹², I. Stan⁶¹, G. Stefanek⁷⁶, M. Steinpreis²⁰, E. Stenlund³⁴, G. Steyn⁶⁴, J.H. Stiller⁹², D. Stocco¹¹², P. Strmen³⁸, A.A.P. Suaide¹¹⁸, T. Sugitate⁴⁶, C. Suire⁵⁰, M. Suleymanov¹⁶, R. Sultanov⁵⁷, M. Šumbera⁸², T.J.M. Symons⁷³, A. Szabo³⁸, A. Szanto de Toledo¹¹⁸, I. Szarka³⁸, A. Szczepankiewicz³⁶, M. Szymanski¹³², J. Takahashi¹¹⁹, N. Tanaka¹²⁶, M.A. Tangaro³³, J.D. Tapia Takaki^{50,ii}, A. Tarantola Pelsoni⁵², M. Tariq¹⁹, M.G. Tarzila⁷⁷, A. Tauro³⁶, G. Tejeda Muñoz², A. Telesca³⁶, K. Terasaki¹²⁵, C. Terrevoli^{30,25}, B. Teyssier¹²⁸, J. Thäder^{96,73}, D. Thomas¹¹⁶, R. Tieulent¹²⁸, A.R. Timmins¹²⁰, A. Toia⁵², S. Trogolo¹¹⁰, V. Trubnikov³, W.H. Trzaska¹²¹, T. Tsuji¹²⁵, A. Tumkin⁹⁸, R. Turrisi¹⁰⁷, T.S. Tveter²², K. Ullaland¹⁸, A. Uras¹²⁸, G.L. Usai²⁵, A. Utrobicic¹²⁷, M. Vajzer⁸², M. Vala⁵⁸, L. Valencia Palomo⁶⁹, S. Vallero²⁷, J. Van Der Maarel⁵⁶, J.W. Van Hoorne³⁶, M. van Leeuwen⁵⁶, T. Vanat⁸², P. Vande Vyvre³⁶, D. Varga¹³⁴, A. Vargas², M. Vargyas¹²¹, R. Varma⁴⁷, M. Vasileiou⁸⁷, A. Vasiliev⁹⁹, A. Vauthier⁷⁰, V. Vechernin¹²⁹, A.M. Veen⁵⁶, M. Veldhoen⁵⁶, A. Velure¹⁸, M. Venaruzzo⁷², E. Vercellin²⁷, S. Vergara Limón², R. Vernet⁸, M. Verweij¹³³, L. Vickovic¹¹⁴, G. Viesti^{30,i}, J. Viinikainen¹²¹, Z. Vilakazi¹²⁴, O. Villalobos Baillie¹⁰¹, A. Vinogradov⁹⁹, L. Vinogradov¹²⁹, Y. Vinogradov⁹⁸, T. Virgili³¹, V. Vislavicius³⁴, Y.P. Viyogi¹³⁰, A. Vodopyanov⁶⁵, M.A. Völkl⁹², K. Voloshin⁵⁷, S.A. Voloshin¹³³, G. Volpe^{36,134}, B. von Haller³⁶, I. Vorobyev⁹¹, D. Vranic^{96,36}, J. Vrláková⁴⁰, B. Vulpescu⁶⁹, A. Vyushin⁹⁸, B. Wagner¹⁸, J. Wagner⁹⁶, H. Wang⁵⁶, M. Wang^{7,112}, Y. Wang⁹², D. Watanabe¹²⁶, M. Weber³⁶, S.G. Weber⁹⁶, J.P. Wessels⁵³, U. Westerhoff⁵³, J. Wiechula³⁵, J. Wikne²², M. Wilde⁵³, G. Wilk⁷⁶, J. Wilkinson⁹², M.C.S. Williams¹⁰⁴, B. Windelband⁹², M. Winn⁹², C.G. Yaldo¹³³, Y. Yamaguchi¹²⁵, H. Yang⁵⁶, P. Yang⁷, S. Yano⁴⁶, Z. Yin⁷, H. Yokoyama¹²⁶, I.-K. Yoo⁹⁵, V. Yurchenko³, I. Yushmanov⁹⁹, A. Zaborowska¹³², V. Zaccolo⁷⁹, A. Zaman¹⁶, C. Zampolli¹⁰⁴, H.J.C. Zanoli¹¹⁸, S. Zaporozhets⁶⁵, A. Zarochentsev¹²⁹, P. Závada⁵⁹, N. Zaviyalov⁹⁸, H. Zbroszczyk¹³², I.S. Zgura⁶¹, M. Zhalov⁸⁴, H. Zhang⁷, X. Zhang⁷³, Y. Zhang⁷, C. Zhao²², N. Zhigareva⁵⁷, D. Zhou⁷, Y. Zhou⁵⁶, Z. Zhou¹⁸, H. Zhu⁷, J. Zhu^{7,112}, X. Zhu⁷, A. Zichichi^{12,28}, A. Zimmermann⁹², M.B. Zimmermann^{53,36}, G. Zinovjev³, M. Zyzak⁴²

¹ A.I. Alikhanyan National Science Laboratory (Yerevan Physics Institute) Foundation, Yerevan, Armenia

² Benemérita Universidad Autónoma de Puebla, Puebla, Mexico

³ Bogolyubov Institute for Theoretical Physics, Kiev, Ukraine

⁴ Bose Institute, Department of Physics and Centre for Astroparticle Physics and Space Science (CAPSS), Kolkata, India

⁵ Budker Institute for Nuclear Physics, Novosibirsk, Russia

⁶ California Polytechnic State University, San Luis Obispo, CA, United States

⁷ Central China Normal University, Wuhan, China

⁸ Centre de Calcul de l'IN2P3, Villeurbanne, France

⁹ Centro de Aplicaciones Tecnológicas y Desarrollo Nuclear (CEADEN), Havana, Cuba

¹⁰ Centro de Investigaciones Energéticas Medioambientales y Tecnológicas (CIEMAT), Madrid, Spain

¹¹ Centro de Investigación y de Estudios Avanzados (CINVESTAV), Mexico City and Mérida, Mexico

¹² Centro Fermi – Museo Storico della Fisica e Centro Studi e Ricerche "Enrico Fermi", Rome, Italy

¹³ Chicago State University, Chicago, IL, United States

¹⁴ China Institute of Atomic Energy, Beijing, China

¹⁵ Commissariat à l'Energie Atomique, IRFU, Saclay, France

¹⁶ COMSATS Institute of Information Technology (CIIT), Islamabad, Pakistan

¹⁷ Departamento de Física de Partículas and IGFAE, Universidad de Santiago de Compostela, Santiago de Compostela, Spain

¹⁸ Department of Physics and Technology, University of Bergen, Bergen, Norway

¹⁹ Department of Physics, Aligarh Muslim University, Aligarh, India

²⁰ Department of Physics, Ohio State University, Columbus, OH, United States

²¹ Department of Physics, Sejong University, Seoul, South Korea

²² Department of Physics, University of Oslo, Oslo, Norway

²³ Dipartimento di Elettrotecnica ed Elettronica del Politecnico, Bari, Italy

²⁴ Dipartimento di Fisica dell'Università 'La Sapienza' and Sezione INFN, Rome, Italy

²⁵ Dipartimento di Fisica dell'Università and Sezione INFN, Cagliari, Italy

²⁶ Dipartimento di Fisica dell'Università and Sezione INFN, Trieste, Italy

²⁷ Dipartimento di Fisica dell'Università and Sezione INFN, Turin, Italy

²⁸ Dipartimento di Fisica e Astronomia dell'Università and Sezione INFN, Bologna, Italy

²⁹ Dipartimento di Fisica e Astronomia dell'Università and Sezione INFN, Catania, Italy

³⁰ Dipartimento di Fisica e Astronomia dell'Università and Sezione INFN, Padova, Italy

³¹ Dipartimento di Fisica 'E.R. Caianiello' dell'Università and Gruppo Collegato INFN, Salerno, Italy

³² Dipartimento di Scienze e Innovazione Tecnologica dell'Università del Piemonte Orientale and Gruppo Collegato INFN, Alessandria, Italy

³³ Dipartimento Interateneo di Fisica 'M. Merlin' and Sezione INFN, Bari, Italy

³⁴ Division of Experimental High Energy Physics, University of Lund, Lund, Sweden

³⁵ Eberhard Karls Universität Tübingen, Tübingen, Germany

³⁶ European Organization for Nuclear Research (CERN), Geneva, Switzerland

³⁷ Faculty of Engineering, Bergen University College, Bergen, Norway

- 38 Faculty of Mathematics, Physics and Informatics, Comenius University, Bratislava, Slovakia
- 39 Faculty of Nuclear Sciences and Physical Engineering, Czech Technical University in Prague, Prague, Czech Republic
- 40 Faculty of Science, P.J. Šafárik University, Košice, Slovakia
- 41 Faculty of Technology, Buskerud and Vestfold University College, Vestfold, Norway
- 42 Frankfurt Institute for Advanced Studies, Johann Wolfgang Goethe-Universität Frankfurt, Frankfurt, Germany
- 43 Gangneung-Wonju National University, Gangneung, South Korea
- 44 Gauhati University, Department of Physics, Guwahati, India
- 45 Helsinki Institute of Physics (HIP), Helsinki, Finland
- 46 Hiroshima University, Hiroshima, Japan
- 47 Indian Institute of Technology Bombay (IIT), Mumbai, India
- 48 Indian Institute of Technology Indore, Indore (IITI), India
- 49 Inha University, Incheon, South Korea
- 50 Institut de Physique Nucléaire d'Orsay (IPNO), Université Paris-Sud, CNRS-IN2P3, Orsay, France
- 51 Institut für Informatik, Johann Wolfgang Goethe-Universität Frankfurt, Frankfurt, Germany
- 52 Institut für Kernphysik, Johann Wolfgang Goethe-Universität Frankfurt, Frankfurt, Germany
- 53 Institut für Kernphysik, Westfälische Wilhelms-Universität Münster, Münster, Germany
- 54 Institut Pluridisciplinaire Hubert Curien (IPHC), Université de Strasbourg, CNRS-IN2P3, Strasbourg, France
- 55 Institute for Nuclear Research, Academy of Sciences, Moscow, Russia
- 56 Institute for Subatomic Physics of Utrecht University, Utrecht, Netherlands
- 57 Institute for Theoretical and Experimental Physics, Moscow, Russia
- 58 Institute of Experimental Physics, Slovak Academy of Sciences, Košice, Slovakia
- 59 Institute of Physics, Academy of Sciences of the Czech Republic, Prague, Czech Republic
- 60 Institute of Physics, Bhubaneswar, India
- 61 Institute of Space Science (ISS), Bucharest, Romania
- 62 Instituto de Ciencias Nucleares, Universidad Nacional Autónoma de México, Mexico City, Mexico
- 63 Instituto de Física, Universidad Nacional Autónoma de México, Mexico City, Mexico
- 64 iThemba LABS, National Research Foundation, Somerset West, South Africa
- 65 Joint Institute for Nuclear Research (JINR), Dubna, Russia
- 66 Konkuk University, Seoul, South Korea
- 67 Korea Institute of Science and Technology Information, Daejeon, South Korea
- 68 KTO Karatay University, Konya, Turkey
- 69 Laboratoire de Physique Corpusculaire (LPC), Clermont Université, Université Blaise Pascal, CNRS-IN2P3, Clermont-Ferrand, France
- 70 Laboratoire de Physique Subatomique et de Cosmologie, Université Grenoble-Alpes, CNRS-IN2P3, Grenoble, France
- 71 Laboratori Nazionali di Frascati, INFN, Frascati, Italy
- 72 Laboratori Nazionali di Legnaro, INFN, Legnaro, Italy
- 73 Lawrence Berkeley National Laboratory, Berkeley, CA, United States
- 74 Lawrence Livermore National Laboratory, Livermore, CA, United States
- 75 Moscow Engineering Physics Institute, Moscow, Russia
- 76 National Centre for Nuclear Studies, Warsaw, Poland
- 77 National Institute for Physics and Nuclear Engineering, Bucharest, Romania
- 78 National Institute of Science Education and Research, Bhubaneswar, India
- 79 Niels Bohr Institute, University of Copenhagen, Copenhagen, Denmark
- 80 Nikhef, National Institute for Subatomic Physics, Amsterdam, Netherlands
- 81 Nuclear Physics Group, STFC Daresbury Laboratory, Daresbury, United Kingdom
- 82 Nuclear Physics Institute, Academy of Sciences of the Czech Republic, Řež u Prahy, Czech Republic
- 83 Oak Ridge National Laboratory, Oak Ridge, TN, United States
- 84 Petersburg Nuclear Physics Institute, Gatchina, Russia
- 85 Physics Department, Creighton University, Omaha, NE, United States
- 86 Physics Department, Panjab University, Chandigarh, India
- 87 Physics Department, University of Athens, Athens, Greece
- 88 Physics Department, University of Cape Town, Cape Town, South Africa
- 89 Physics Department, University of Jammu, Jammu, India
- 90 Physics Department, University of Rajasthan, Jaipur, India
- 91 Physik Department, Technische Universität München, Munich, Germany
- 92 Physikalisches Institut, Ruprecht-Karls-Universität Heidelberg, Heidelberg, Germany
- 93 Politecnico di Torino, Turin, Italy
- 94 Purdue University, West Lafayette, IN, United States
- 95 Pusan National University, Pusan, South Korea
- 96 Research Division and ExtreMe Matter Institute EMMI, GSI Helmholtzzentrum für Schwerionenforschung, Darmstadt, Germany
- 97 Rudjer Bošković Institute, Zagreb, Croatia
- 98 Russian Federal Nuclear Center (VNIIEF), Sarov, Russia
- 99 Russian Research Centre Kurchatov Institute, Moscow, Russia
- 100 Saha Institute of Nuclear Physics, Kolkata, India
- 101 School of Physics and Astronomy, University of Birmingham, Birmingham, United Kingdom
- 102 Sección Física, Departamento de Ciencias, Pontificia Universidad Católica del Perú, Lima, Peru
- 103 Sezione INFN, Bari, Italy
- 104 Sezione INFN, Bologna, Italy
- 105 Sezione INFN, Cagliari, Italy
- 106 Sezione INFN, Catania, Italy
- 107 Sezione INFN, Padova, Italy
- 108 Sezione INFN, Rome, Italy
- 109 Sezione INFN, Trieste, Italy
- 110 Sezione INFN, Turin, Italy
- 111 SSC IHEP of NRC Kurchatov institute, Protvino, Russia
- 112 SUBATECH, Ecole des Mines de Nantes, Université de Nantes, CNRS-IN2P3, Nantes, France
- 113 Suranaree University of Technology, Nakhon Ratchasima, Thailand
- 114 Technical University of Split FESB, Split, Croatia
- 115 The Henryk Niewodniczanski Institute of Nuclear Physics, Polish Academy of Sciences, Cracow, Poland
- 116 The University of Texas at Austin, Physics Department, Austin, TX, United States

- ¹¹⁷ *Universidad Autónoma de Sinaloa, Culiacán, Mexico*
- ¹¹⁸ *Universidade de São Paulo (USP), São Paulo, Brazil*
- ¹¹⁹ *Universidade Estadual de Campinas (UNICAMP), Campinas, Brazil*
- ¹²⁰ *University of Houston, Houston, TX, United States*
- ¹²¹ *University of Jyväskylä, Jyväskylä, Finland*
- ¹²² *University of Liverpool, Liverpool, United Kingdom*
- ¹²³ *University of Tennessee, Knoxville, TN, United States*
- ¹²⁴ *University of the Witwatersrand, Johannesburg, South Africa*
- ¹²⁵ *University of Tokyo, Tokyo, Japan*
- ¹²⁶ *University of Tsukuba, Tsukuba, Japan*
- ¹²⁷ *University of Zagreb, Zagreb, Croatia*
- ¹²⁸ *Université de Lyon, Université Lyon 1, CNRS/IN2P3, IPN-Lyon, Villeurbanne, France*
- ¹²⁹ *V. Fock Institute for Physics, St. Petersburg State University, St. Petersburg, Russia*
- ¹³⁰ *Variable Energy Cyclotron Centre, Kolkata, India*
- ¹³¹ *Vinča Institute of Nuclear Sciences, Belgrade, Serbia*
- ¹³² *Warsaw University of Technology, Warsaw, Poland*
- ¹³³ *Wayne State University, Detroit, MI, United States*
- ¹³⁴ *Wigner Research Centre for Physics, Hungarian Academy of Sciences, Budapest, Hungary*
- ¹³⁵ *Yale University, New Haven, CT, United States*
- ¹³⁶ *Yonsei University, Seoul, South Korea*
- ¹³⁷ *Zentrum für Technologietransfer und Telekommunikation (ZTT), Fachhochschule Worms, Worms, Germany*

ⁱ Deceased.

ⁱⁱ Also at: University of Kansas, Lawrence, Kansas, United States.